Beyond MAGT: learning more from permafrost thermal monitoring data with additional metrics

Nicholas Brown[1,2] and Stephan Gruber[1]

[1]Department of Geography and Environmental Studies, Carleton University, Ottawa, Canada
[2]NSERC PermafrostNet, Carleton University, Ottawa, Canada

Correspondence: Nick Brown (nick.brown@carleton.ca)

Abstract. Metrics such as the mean annual ground temperature (MAGT) and active layer thickness (ALT) are used to monitor and quantify permafrost change. However, these have limitations including those arising from the effects of latent heat, which reduce their sensitivity. We investigated the behaviour of existing and novel metrics derived from temperature observations (TSP metrics) using an ensemble of more than seventy 120-year simulations. We evaluated which TSP metrics provide new insight into permafrost change and evaluated how reliably each one indicates changes in sensible, latent, and total heat contents for different levels of sensor quality. We also quantified the effect of sensor placement on the magnitude of observed MAGT trends.

Based on this, we recommend a parsimonious set of five TSP metrics that provide a better picture of permafrost thaw than MAGT alone. These are: height of the permafrost table (TOP), depth of zero annual amplitude (d_{za}), thermal integral ($\bar{\tau}$), mean annual ground temperature (MAGT), and mean annual surface temperature (MAGST).

We observed depth-related differences in MAGT warming rates of more than 0.23 °C dec^{-1} in 50% of 10-year observation periods for observation depths between 10 m and 20 m. The magnitude of these differences roughly corresponds to the mean warming rate reported for discontinuous permafrost. The effect of sensor depth on warming trends is found to be greatest in ice-poor soils. These results illustrate the challenge of interpreting the magnitude of observed ground temperature trends.

Our results can be used to inform permafrost monitoring strategies and help contextualize observed trends. Consistent metrics can be produced from observed and simulated thermal data via the "tspmetrics" library available on the Python Package Index (PyPi).

1 Introduction

Permafrost is an important component of the global climate system (IPCC, 2022) and its changes affect ecosystems, infrastructure, and ways of life in high-latitude (Meredith et al., 2019) and mountainous (Hock et al., 2019) regions. Ground temperature is the most common variable in permafrost monitoring and one of three products used to characterize the permafrost Essential Climate Variable by the World Meteorological Organization (Sessa and Dolman, 2008; Smith and Brown, 2009). Temperatures are usually recorded at discrete depths in boreholes with thermistor chains and data loggers. The way in which the resulting T(z, t) data, i.e., temperature at different depths (z) and times (t), are processed into summary metrics determines what conclu-

25 sions can be drawn during interpretation and what value can be derived from the investment in thermal monitoring. We argue that current practices for processing and reporting permafrost thermal monitoring data overlook important information and can be improved by including additional metrics.

To conceptualize the utility of differing metrics, common uses of ground temperature monitoring data can be grouped by the relevance of changes in three key quantities: (1) sensible heat content (H_s), which directly reflects temperature changes.

30 Temperature also reveals whether the definition of permafrost—soil or rock below 0 °C for more than two consecutive years—is met; (2) latent heat content (H_l), which reflects the melting or formation of ground ice; (3) total heat content (H_t), which is the sum of sensible and latent heat content and is relevant for subsurface heat storage (Cuesta-Valero et al., 2022; Von Schuckmann et al., 2023). The latent heat content is the most important quantity from the perspective of hazards and adaptation because changes in the ice content are closely related to landscape change, slope instability, hydrology, contaminant mobility, and

35 ecosystem changes.

Most often, long-term changes in permafrost are described using the mean annual ground temperature (MAGT) measured near the depth of zero annual amplitude (d_{za}) where the annual temperature amplitude is dampened to less than 0.1 °C (e.g., Romanovsky et al., 2010). These observations typically use temperature measurements from a single sensor 10–25 m deep, where some of the temporal and spatial variability present at shallower depths is smoothed out. Inferring permafrost change

40 using MAGT trends at single depths of 10–25 m alone, however, entails five major shortcomings:

(1) Latent heat changes are hidden ('latent') in temperature observations. We can see this where MAGT series flatlining just below 0 °C are shown and figure captions suggest a counterintuitive and ambiguous interpretation: that such periods with barely visible change in fact indicate fast ice loss in the ground (cf. Smith et al., 2010; Groenke et al., 2022).

(2) MAGT changes are inconsistent temporally and spatially as a result of differences in the partitioning of latent and sensible

45 heat. Temporally, the same temperature change at the ground surface can cause a strong MAGT response in cold permafrost but after years of warming only cause minute MAGT change when the borehole is close to 0 °C. Spatially, a borehole in ground with little ice may be warming fast while a nearby borehole in ice-rich ground may warm only slowly. This inherent inconsistency of the MAGT confounds spatial and temporal comparison, even though such comparisons are common (e.g. Smith et al., 2022; Biskaborn et al., 2019). Moreover, the sampling of locations for making boreholes in a region is known to

50 often be biased towards sites that are accessible, likely to contain permafrost, of scientific or practical interest, or in ground materials amenable to drilling (e.g. Noetzli et al., 2021; Biskaborn et al., 2019; Subedi et al., 2020). Such bias will affect average warming rates in a region, further obscuring any meaning that can be derived from averages.

(3) Differences in observed depth can further affect the relative timing and magnitude of the MAGT trends from different locations. There is no standardized measurement depth near d_{za} in the current practice of reporting MAGT and the potential

55 magnitude of depth-related effects is unknown.

(4) Relying on MAGT alone forgoes valuable information that is usually recorded at other depths. Although MAGT provides direct insight into the thermal state of the ground at a specific depth, it masks changes occurring elsewhere in the soil profile and offers limited information about the physical processes and hazards associated with permafrost thaw, which often occurs closer to the ground surface.

60   (5) Deep boreholes are rare. Observation at or near d_{za} is useful as a single statistic, however, restricting ourselves to boreholes of 10 m or more neglects a great deal of data. Metrics suitable also for shallower boreholes are therefore desirable, especially when considering the paucity of published ground temperature data (Brown et al., 2024). Data loggers easily produce annual average temperatures, overcoming the historic requirement of observation near d_{za} to avoid aliasing in episodic manual observation.

65   In summary, these five shortcomings mean that using MAGT as the sole indicator of permafrost change presents an interpretation challenge, as its magnitude is not consistently proportional to any single property of interest. Furthermore, using only MAGT (a common practice with some notable exceptions, e.g., PERMOS, 2021) ignores most of the available $T(z,t)$ data that is collected at great expense.

With the goal of informing decision-making and permafrost research (cf. Gruber et al., 2023), we aim to better use $T(z,t)$
70   observations for revealing permafrost change by complementing MAGT. We denote *TSP metrics* as summary numbers representing the annual thermal state of permafrost that are derived from $T(z,t)$ data.

The objectives of this study are to: (1) Review and develop TSP metrics, formalizing their calculation where necessary. (2) Quantify the effect of MAGT sensor depth on observed warming rates. (3) Evaluate how well TSP metrics reflect sensible, latent, and total heat gains in permafrost using simulated observations. (4) Recommend a parsimonious set of TSP metrics for
75   future use. (5) Demonstrate the utility of the metrics recommended with example data from the GTN-P database.

We proceed by reviewing published metrics and proposing new ones. Then, the behaviour of metrics is empirically tested with an ensemble of 120-year time series of simulated transient ground temperatures. In these simulations, not only the temperatures, but also the sensible, latent, and total heat contents in the soil column are known. Metrics can thus be evaluated in their ability to represent their changes. While this methodology cannot support firm conclusions about all possible configurations of
80   ground and climate, it does provide an opportunity for knowledge generation beyond what current field data alone cannot offer.

2   TSP metrics

Many techniques exist to interpret permafrost change from ground temperature records. Some are formalized and quantitative (e.g., MAGT) while others involve a qualitative interpretation (e.g., the development of isothermal conditions). Although temperature is our sole input variable, we aim to gain additional insight into the effects of latent heat.

85   The metrics presented here (Table 1) produce annual summary values. They are derived from ground temperature observations reported for constant depths relative to the ground surface. In practice, ground subsidence may result in sensor depths that change over time. Most metrics are calculated from multiple sensors to represent an entire soil column and location. Only MAGT is based on a single sensor that must be selected. Where available, we also discuss observed rates of change for these metrics from existing monitoring efforts or other studies.

2.1 Mean Annual Ground Temperature (MAGT)

Measuring trends in MAGT is one of the most common ways to quantify permafrost change. The measurement of ground temperatures at or near d_{za} is established practice and effective at smoothing out inter-annual and fine-scale spatial variability. Typically, permafrost warming trends are calculated from sensors 10–25 m deep using linear regression of temperature time series (Isaksen et al., 2007; Smith et al., 2022) or Bayesian methods (Groenke et al., 2022).

We distinguish between MAGT measured at a specific fixed depth (denoted T_d at depth d) and mean annual ground temperature measured at the true d_{za}, the position of which is dynamic over time. We denote this latter metric T_{za} and discuss it below.

Observed rates of MAGT change are typically lower than 0.3 °C dec^{-1} for warm permafrost (>-2 °C) and lower than 1 °C dec^{-1} for cold permafrost (<-2 °C) (Smith et al., 2022). Biskaborn et al. (2019) estimated average warming rates as 0.39 °C dec^{-1} in continuous permafrost, 0.20 °C dec^{-1} in discontinuous permafrost, and 0.29 °C dec^{-1} globally.

2.2 Mean Annual Ground Surface Temperature (MAGST)

MAGSTs provide information on changes to the upper boundary of a soil column, which propagate downwards to affect permafrost. Because they do not require costly drilling, MAGST measurements can be collected more economically than thermistor strings in boreholes, and enable denser data collection (e.g. Brown et al., 2022; Gruber et al., 2003). We calculate MAGST using model output at 0.1 m.

Systematic reporting of MAGST is less common than for MAGT or active layer thickness at permafrost research sites (Wang et al., 2024). In Switzerland, MAGST warming rates over permafrost have been estimated as 0.4–0.6 °C dec^{-1} (1998–2022, Swiss Permafrost Monitoring Network, 2024). On the Tibetan Plateau, MAGST warming rates were estimated as 0.16–0.60 °C dec^{-1} (1980–2015, Hu et al., 2019) and 0.60 °C dec^{-1} on average (1980–2007, Wu et al., 2012). Average trends across China (including non-permafrost regions) were reported as 0.20 ± 0.02 °C dec^{-1} (1956–2022, Wang et al., 2024).

2.3 Active layer thickness (ALT)

ALT is one of three products used to monitor the permafrost Essential Climate Variable (Hu et al., 2025; Sessa and Dolman, 2008). Strictly speaking, its vertical extent is defined by the the greatest thaw penetration depth in a year, the maximum extent of the zero-degree isotherm is sometimes used as a thermal approximation of the active layer (Bonnaventure and Lamoureux, 2013). The thermally defined ALT has the advantage that it can be estimated using ground temperature records. This is often done by interpolating the two observations above and below the active layer (Streletskiy et al., 2017; Nelson and Hinkel, 2003). However, Riseborough (2008) found that the lowest error (equal to about 20% of node spacing) was obtained by extrapolating from above using the two lowest sensors in the active layer, and by using instantaneous profiles rather than annual envelopes. The worst results were obtained when extrapolating from measurements below the active layer. Alternatively, some authors suggest fitting exponential curves to the ground temperature envelope (Nelson and Hinkel, 2003).

To estimate active layer thickness using the 'extrapolation from above' method described by (Riseborough, 2008), we first calculate annual maximum temperatures at each sensor depth and identify the index (n) of the deepest sensor above permafrost where temperatures exceed 0 °C during the year.

Next, for each time step we determine the extrapolated thermal gradient using the deepest (z_n) and second-deepest (z_{n-1}) sensors above the isotherm

$$\frac{dT}{dz}(t) = \frac{T(z_n, t) - T(z_{n-1}, t)}{z_n - z_{n-1}}.$$
(1)

The depth intercept of the zero-degree isotherm is then calculated as follows:

$$z_{T=0}(t) = z_n + \frac{0 - T(z_n, t)}{\frac{dT}{dz}(t)}.$$
(2)

Next, the process is repeated, but using the deepest sensor above permafrost with minimum temperature below 0 °C. This is repeated for all time steps in the year, and the active layer thickness is chosen as the greatest depth intercept

$$ALT^{\downarrow} = max\{z_{T=0}(t_1)...z_{T=0}(t_i)\}.$$
(3)

To estimate ALT by interpolation ($ALT^{\updownarrow}$), we use a similar approach, but calculate the thermal gradient using the nth and $(n+1)^{st}$ sensors. Additionally, the position of the permafrost table can also be estimated by using only the maximum temperature in Equations 1 and 2. Finally, we average the two estimates of ALT

$$ALT = \frac{1}{2}(ALT^{\updownarrow} + ALT^{\downarrow}).$$
(4)

Long-term trends in ALT provide a minimum estimate for how much permafrost is lost due to thaw, but are insensitive to any additional ground lost due to thaw subsidence (O'Neill et al., 2023).

Observed ALT trends are typically low. Data from 109 active layer monitoring sites shows rates of increase generally between -0.2 to +0.4 m dec^{-1} depending on the region, but up to +3.9 m dec^{-1} in the Swiss Alps (Smith et al., 2022).

2.4 Height of the permafrost table (TOP)

In cold permafrost, our estimate of the ALT coincides with the depth to the permafrost table, or top of permafrost (TOP). However, the potential development of a supra-permafrost talik causes these two metrics to differ by an amount roughly equal to the talik thickness (neglecting any differences between the thermal and physical boundaries of taliks and active layer).

It is possible for TOP to change independently of ALT, so we consider TOP as an additional metric. To calculate TOP we use Equations 1 and 2 to estimate the position of the zero-degree isotherm.

2.5 Annual thaw-depth duration ($\bar{D}$)

While change to ALT is commonly used as an indicator of thaw (Brown et al., 2000), it does not include any information about the duration of thaw. Both factors have implications for biological activity, terrain hazards, and carbon cycling. Harp et al.

(2016) define ($\bar{\mathcal{D}}$), a time- and depth-integrated value as

150
$$\bar{\mathcal{D}} = \frac{1}{365} \iint H(T(z,t))dzdt, \tag{5}$$

where T(z,t) describes the mean soil temperature at an arbitrary depth (m) and time (d). For each year, we select integration bounds from the ground surface to the top of permafrost, and from 0 to 365 days (simulations do not consider leap years). Here, H is the Heaviside step function:

$$H(T) = \begin{cases} 0, & T \leq 0 \\ 1, & T > 0 \end{cases}$$

155 Practically, for daily observational data, we use a discretized form of this equation

$$\bar{\mathcal{D}} = \frac{1}{365} \sum_{j=1}^{365} \sum_{i=1}^{N} H(\tau(z_i, t_j)) \Delta z. \tag{6}$$

Here τ is a linearly interpolated function of temperature with depth, discretized into N elements, and Δz is an arbitrary thickness increment, for which we use 0.01 m. Note that the use of interpolation rather than extrapolation across the zero-degree isotherm at the thaw depth may introduce a slight bias here (Hinkel, 1997).

160 **2.6 Depth of Zero Annual Amplitude (d_{za})**

The depth at which the annual temperature amplitude is completely attenuated is denoted (d_{za}). A cutoff value of 0.1 °C in amplitude is typically used as a practical threshold.

Intuitively, we expect that d_{za} will be shallower for boreholes in which greater amounts of thaw take place, and in ice-rich boreholes where seasonal freezing and thawing decrease the apparent thermal diffusivity. This latter case indicates a greater
165 *potential* for thaw. Over longer periods of time, increasing d_{za} should be expected to indicate a change to an increasingly latent heat-dominated system.

To estimate d_{za} we use the method described by Bonnaventure et al. (2015). Additional considerations for this calculation are described in Appendix E. First, the annual amplitude A_z at each observation depth, z, is calculated as:

$$A_z = \frac{1}{2}(T_z^{max} - T_z^{min}). \tag{7}$$

170 Next, we fit coefficients x_0 and x_1 using least squares,

$$ln(\frac{\overrightarrow{A}}{A_0}) = x_0 - x_1 \frac{\overrightarrow{Z}}{Z_0}. \tag{8}$$

Where, A_0 and Z_0 are units of 1 °C and 1 m. For this step, we restrict the data by only using depth and amplitude pairs where $A > 0.5\,°C$ so that temperature trends at depth do not add noise by inflating the amplitude. Finally, we calculate d_{za} using the fitted coefficients for each year of data

175
$$\frac{d_{za}}{Z_0} = \frac{x_0 - ln(0.1)}{x_1}. \tag{9}$$

We are not aware of any long-term observations tracking d_{za} change over time. For the most part, d_{za} is treated as a static property to characterize or compare sites.

2.7 Dynamic Mean Annual Ground Temperature at the Depth of Zero Annual Amplitude (T_{za})

Although MAGT is defined as the temperature at the depth of zero annual amplitude, it is typically recorded at a fixed depth
180   below d_{za} in the range of 10 to 25 m.

We calculate a dynamic mean annual temperature at the depth of zero annual amplitude (T_{za}) whose position corresponds
to the best estimate of d_{za} calculated above. After determining d_{za}, we interpolate the MAGT linearly to that depth to obtain
T_{za}. Although this measurement technically describes a single depth, we consider it a borehole-aggregated metric because it is
uniquely defined for any location, there are no choices to be made about its position, and it derives from more than one sensor.

185   As will be shown, T_{za} is the first ground temperature metric to become isothermal, and therefore can be used as a way to
further classify borehole behaviour.

For clarity, we will use the acronym MAGT to refer to mean annual ground temperatures at a *fixed-depth*, and refer explicitly
to T_{za} as necessary.

2.8 Annual Thermal Integral ($\bar{\tau}$)

190   One drawback of monitoring temperature at a single depth is that this neglects a great deal of data, and that warming rates
may differ at other locations in the profile. To investigate an alternative, we define the thermal integral as the depth-integrated
temperature evaluated between a near-surface sensor (a) and an arbitrary depth (b) of the mean annual temperature profile

$$\bar{\tau}_b^a = \frac{1}{(b-a)} \int_b^a T(z)dz. \tag{10}$$

Because we sample temperatures at discrete depths, we estimate thermal integrals from the uppermost to lowermost sensor
195   depths using the trapezoidal rule

$$\bar{\tau}_{z_n}^{z_1} \approx \frac{1}{2(z_n - z_1)} \sum_{i=1}^{n-1} (T(z_i) + T(z_{i+1}))(z_{i+1} - z_i). \tag{11}$$

Where z_i is the depth of the ith sensor. This value is normalized by the integration depth, yielding effectively a mean column
temperature. Trends in the thermal integral correspond to mean column warning rates. Our hypothesis is that the trends are
more comparable between boreholes provided that the total integrated depths are the same. This is because the measurement
200   depth will not differ between boreholes and because results are affected less strongly by the number and spacing of sensors.

3 Methods

3.1 Data pre-processing and conventions

Our processing uses daily $T(z,t)$ data; sub-daily values are aggregated to daily averages first. For each annual period evaluated
with TSP metrics, the number of daily values is reported and we exclude years with less than 95% data completeness. We
205   consider $T(z,t)$ data to be reported for constant depths relative to the ground surface. In practice, ground subsidence may result

Table 1. Summary of TSP metrics used in this study. Data requirements also include sensitivities to missing, biased, or inaccurate data.

Metric	Description	Data requirements
Mean annual ground temperature (MAGT)	Annual mean temperature at a specific observation depth, typically at or below d_{za} (Smith et al., 2022).	Requires sufficiently deep observations. Long-term records affected by sensor drift and changes to sensor depth.
Active layer thickness (ALT)	Thickness of ground above permafrost that freezes and thaws seasonally (Smith et al., 2022; Burn, 1998).	Precision limited by sensor spacing (Riseborough et al., 2008) and by large data gaps.
Height of permafrost table (TOP)	Height of the permafrost table relative to a fixed datum.	Limited by same data requirements as ALT.
Thaw-depth duration ($\bar{\mathcal{D}}$)	Annual time- and depth- integrated duration of temperatures above 0 °C (Harp et al., 2016).	Sensitive to missing data in thawed active layer or talik, but insensitive to missing data at other times and depths.
Depth of zero annual amplitude (d_{za})	Depth where seasonal temperature variation is attenuated to an amplitude of less than 0.1 °C.	Sensitive to sensor noise and to missing data at annual temperature extrema. Interpolation methods require sufficiently deep observations (Bonnaventure et al., 2015).
Mean annual temperature at the dynamic d_{za} (T_{za})	Annual mean temperature at d_{za}.	Requires observations below d_{za}. Requirements of MAGT also apply.
Thermal integral ($\bar{\tau}$)	Depth-integrated mean annual temperature, approximates mean annual borehole temperature.	Requires sensors above and below (or equal to) integration bounds. Sensor spacing affects precision. Sensitive to missing data but impact is diminished by collecting data from multiple sensors.
Mean annual ground surface temperature (MAGST)	Mean annual temperature just beneath the ground surface (< 10cm).	Requirements and sensitivities similar to MAGT but wider annual temperature range increases sensitivity to missing data. Greater interannual variability in MAGST requires longer data to establish meaningful trend. (Hu et al., 2019; Staub et al., 2017; Swiss Permafrost Monitoring Network, 2024)

in sensor depths changing over time. Multi-year trends in TSP metrics are calculated using ordinary least squares regression. For the model experiments, we calculate rolling trend windows of 5-, 10- and 20-year duration, representing data durations commonly available from permafrost monitoring today.

3.2 Quantifying the effect of depth on warming rates

210 We evaluate the effect of observation depth on MAGT trends and compare it to the effect of total integration depth on trends in $\bar{\tau}$. For each trend window, the maximum difference in change rates of all depths between 10 m and 20 m is calculated. For MAGT, this is done in two ways: first, by including all data, and again excluding any depths at which permafrost has degraded completely. Finally, empirical cumulative distribution functions are generated to quantify the effect of observation depth.

3.3 Ground temperature simulation

215 We use the model FreeThawXice1D (Tubini and Gruber, 2025; Tubini et al., 2021) to simulate transient ground temperatures in a one-dimensional configuration. This model represents the effects of subsidence caused by ground-ice loss and accurately tracks 0 °C isotherms via local mesh refinement. We use GlobSim (Cao et al., 2019) to generate meteorological forcing data from the ERA5 reanalysis to drive the model at the upper boundary. This tool streamlines the download of reanalysis data, interpolates grid cells to point-scale to make data suitable for 1D simulation, standardizes units and timesteps, and performs
220 heuristic downscaling to account for terrain and other local effects. Future conditions are simulated by repeating several years of data with an added linear warming trend. More details on the simulation and the evaluation of resulting temperatures are presented in Appendix B.

3.4 Emulating imperfect observation data

Simulation results are near-perfect data, with limitations related to model assumptions and numerical imprecision. To assess
225 the sensitivity of TSP metrics to the quality limitations of real measurement systems, we degrade simulation results accounting for the accuracy (bias), drift, and precision (noise) of typical sensing systems (Appendix C). Based on typical performance characteristics, we create two additional data sets (Table 2) that emulate an excellent ($\mathcal{Q}_1$) and a good ($\mathcal{Q}_2$) commercial measurement system. The original model output is denoted ($\mathcal{Q}_0$).

Table 2. The three levels of data quality: ($\mathcal{Q}_0$) original simulation output, ($\mathcal{Q}_1$) emulating an excellent monitoring system, and ($\mathcal{Q}_2$) emulating a good monitoring system.

	Noise (σ) [mK]	Bias [mK]	Drift [mK yr^{-1}]
$\mathcal{Q}_0$	0	0	0
$\mathcal{Q}_1$	10	± 50	± 1
$\mathcal{Q}_2$	50	± 150	± 10

3.5 Evaluating TSP metrics as indicators of change

230 For each time window, TSP metrics are regressed against the change in heat content (sensible, latent, total). The strength of the relation—represented by the regression slope—is normalized by the standard error. The resulting values for the t-statistic, here analogous to a signal-to-noise ratio, are summarized in a histogram. Histograms are displayed to distinguish regression results by the statistical significance (p < 0.05) and sign of the resulting trend.

The distribution of t-statistics across all trend windows is used as a measure of the reliability of a TSP metric as a way to
235 detect heat-content changes in the ground. Positive slopes indicate true positives (sensitivity when expressed as a rate) and negative slopes indicate false positives (specificity when expressed as a rate). Spuriously significant regression can occur given the non-stationarity of our time series. Because all simulations are subject to similar levels of non-stationarity, the effects on relative efficacy of metrics is likely small.

3.6 Distinguishing stages of permafrost thaw

240 As will be shown below, T_{za} is the first mean temperature metric to reach isothermal behaviour near 0 °C. We investigate whether this metric can be used to partition the simulations into two distinct phases of thaw. For this particular experiment, we exclude bedrock simulations which have no appreciable ice content. For each simulation, we identify the breakpoint in slope (e.g., Figure 1 i) visually. Once the date is established, the mean trend in H_s and H_l are computed for the period before and after. Finally, the relative change in slope is computed as:

245 $$\text{Mean Trend Ratio} = \frac{m_{after}}{m_{before}}, \tag{12}$$

where m is the corresponding mean trend. We also aim to develop a way to automatically determine the date of the breakpoint. For this, we use a quantitative threshold of four consecutive years of less than 0.1 °C of change in T_{za}. Finally, for comparison, we perform the same analysis using the commonly-used criterion to distinguish *warm* permafrost based on MAGT. That is, when MAGT of permafrost is between -2 and 0. We define the boundary as when T_{20} reaches -2 °C for the first time;
250 in our simulations this transition happens before the T_{za} breakpoint.

4 Testing TSP metrics with simulated data

We simulate 120 years of subsurface change and use the resulting output to evaluate the TSP metrics in a physically-consistent setting with access to all variables needed. Reanalysis data from 1980–2022 is used and future scenarios add linear trends on repeated data to extend the dataset to 2100. In this section, we describe the configuration of experiments, present their results,
255 and guide the reader through their interpretation. We first interpret all simulations visually, in particular the behaviour in warm permafrost and redundancy between metrics. Then, we quantitatively compare how well the metrics represent changes in latent, sensible, and total heat content using regression.

In the experiment presented here, meteorological conditions are simulated for three different sets of spatial coordinates. These conditions are varied and extended using fixed offsets and warming trends, respectively (Appendix B). Simulations

260   reflect a variety of surface and subsurface conditions: five different soil profiles are used, spanning conditions from water-free bedrock to fine-grained sediments with excess ice (Table B1). Combined with the different meteorological conditions, this resulted in 75 distinct simulations.

The output is produced with temperature and ice content up to a depth of 25 m (at 0.2, 0.4, 0.8, 1.2, 1.6, 2, 2.5, 3, 3.5, 4, 5, 7, 9, 10, 11, 13, 15, 20 and 25 m, cf. Harris et al., 2009) as well as for the elevation of the ground surface, total ice content,

265   heat content (total, sensible, latent) of the soil column, and the positions of zero-degree isotherms.

4.1   Visual interpretation of example simulations

We present the results of two simulations as exemplars of the simulation ensemble and the behaviour of TSP metrics. The first simulation (Figure 1 a–f) is for a cold soil column containing no excess ice with an initial MAGT near -6 °C. Heat gain throughout the simulation is predominantly through sensible heat and approximately linear in time. All metrics exhibit a

270   similarly linear response.

The second illustrative simulation (Figure 1 g–l) is for a column containing excess ice with an initial MAGT of around -3 °C. The loss of excess ice causes a decreasing ground surface height accompanied by an approximately linear increase in heat content. Unsurprisingly, the warming rate of MAGT is strongly dampened late in the simulation, demonstrating the challenge associated with interpreting this metric in the presence of latent heat transfer.

275   Each TSP metric will be discussed in further detail below. Given the relative simplicity of metrics in cold permafrost, discussion will focus on behaviour in warm and icy permafrost. When available, rates of change from field observations are provided to contextualize simulated data.

4.2   Permafrost thickness: ALT, TOP, and $\bar{D}$

The ALT trend can be positive or negative in warm permafrost. When a talik develops, this causes a discontinuity in ALT

280   followed by a reverse in the direction of the trend (Figure 1 i). This generally occurs in three stages: (1) An initial decoupling of ALT from the permafrost table when the ground no longer refreezes completely and a residual thaw layer persists. (2) A period when ground temperatures near 0 °C and multi-year temperature variability cause ALT to vary strongly, with occasional large jumps. (3) A more stable period (not shown in Figure 1 g–l) during which ALT decreases once the talik is well developed. ALT thinning has also been observed in the field (Connon et al., 2018).

285   In contrast to ALT, TOP declines monotonically during the warming period, indicating the loss of permafrost volume with less ambiguity as it is not reversing with the formation of a talik. Similarly, $\bar{D}$ is monotonic in its reaction to sustained warming. For the remaining analysis, we use TOP as the metric of choice, intuitively summarizing changes to the upper boundary of permafrost. Before the formation of a talik, changes in TOP, ALT, and $\bar{D}$ are very similar. This is not surprising given the considerable overlap between the definitions of these three metrics.
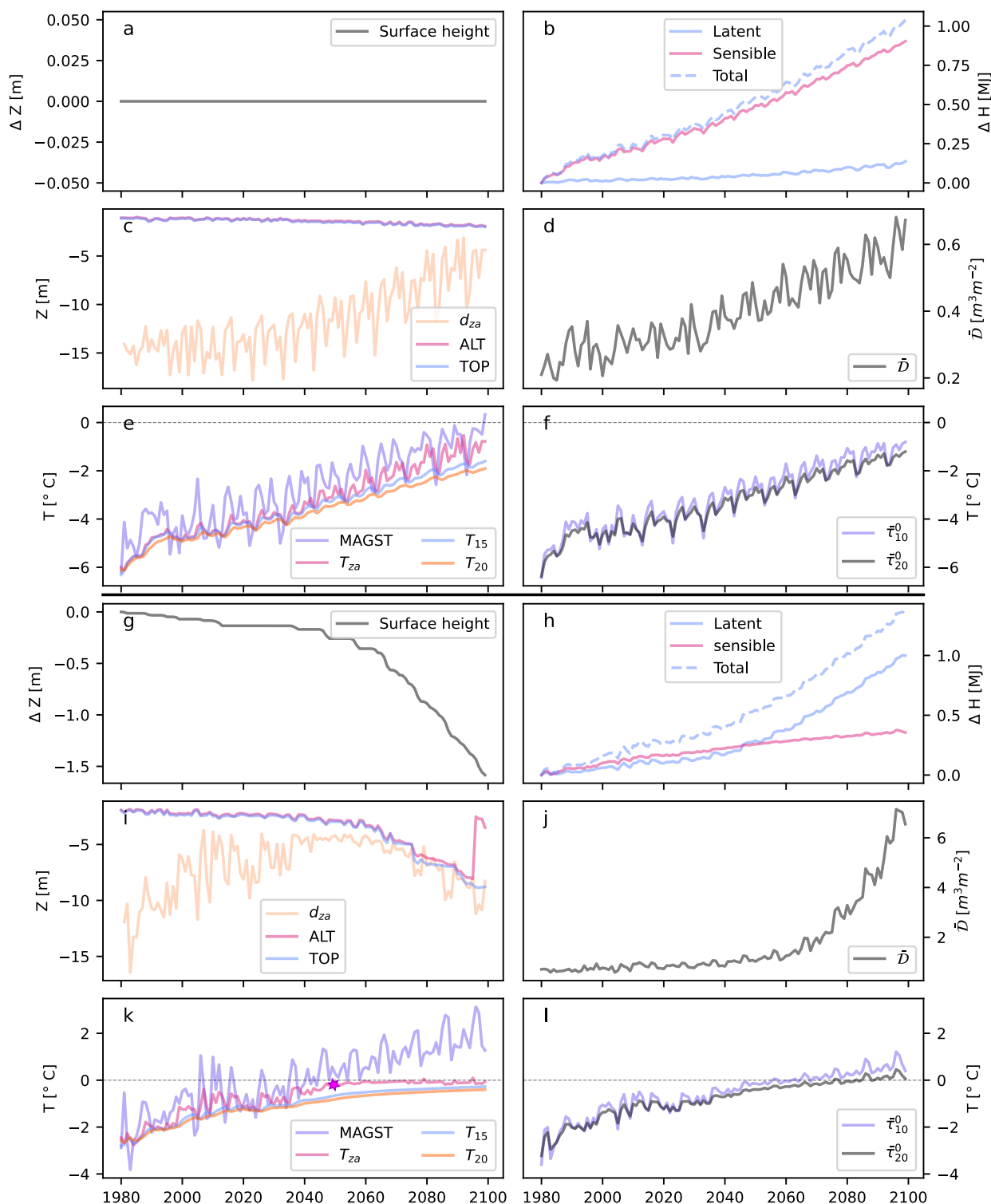
Figure 1. Warm and icy permafrost (g–l) exhibits much more nonlinear trends than cold permafrost (a–f) in metrics, surface height and heat content. Simulations allow us to visually compare different metrics. Here, we present 120 years of warming and the corresponding evolution of permafrost metrics for a cold simulation containing no excess ice (a–f) and for a warm simulation containing excess ice (g–l). Periodic variation from 2022 onward is due to the repetition of reanalysis data used to drive the simulation. In subplot (i), the purple star indicates the breakpoint in T_{za} when it becomes isothermal.

12

290   In warm simulations, we see that ALT, $\bar{\mathcal{D}}$, and TOP change gradually for some time and then the rate of change begins to increase dramatically. This regime change between cold and warm permafrost has been previously described (Changwei et al., 2015; Wu and Zhang, 2010).

4.3   MAGT and T_{za}

Visually, MAGT behaves most similarly to borehole sensible heat content until it nears 0 °C, when warming rates decline in
295   simulations with ground ice. Trends in T_{za} are similar to those of MAGT. However, in warming simulations with ice, T_{za} is the first depth to become near-isothermal because d_{za} becomes shallower as phase change takes place and temperature fluctuations are damped by latent heat transfer. The magnitudes of simulated trends in T_{za} and MAGT are similar.

In cold or moisture-poor permafrost, MAGT and T_{za} both generally follow a similar pattern as H_s. It is the effect of latent heat near 0 °C that dampens the warming trend in other cases. Because T_{za} is the first metric to reach isothermal behaviour,
300   it is a good candidate for an additional metric. T_{za} also does not involve an arbitrary choice of depth but is derived from the behaviour of all observations. Otherwise, observations at a fixed depth, as commonly used for MAGT, are preferable to T_{za} becasue they are simpler to produce and understand.

4.3.1   Distinguishing stages of thaw

When simulations are partitioned into warm (MAGT $\geq -2°C$) and cold (MAGT $< -2°C$) permafrost, the mean H_l trend is
305   significantly greater in warm permafrost than in cold permafrost (Figure 2). This is not true of the H_s trend, for which the 95% confidence interval of the mean trend ratio includes 1. On the other hand, when using a visually picked breakpoint in T_{za} (e.g., Figure 1 i) to distinguish two stages of thaw, we see that H_l trends are significantly greater in the later stages of thaw and H_s are significantly reduced. This is also true when the T_{za} breakpoint is estimated quantitatively rather than visually.

Another advantage of the T_{za} classification is that, because no specific depth must be chosen, the classification is valid for
310   the entire borehole. Since d_{za} moves towards the surface, it also more likely that when the transition from one stage to another takes place, the sensors will be placed deep enough to measure this.

While we generally expect H_s trends to decrease and H_l trends to increase as icy permafrost warms, the choice of where to split up different stages of thaw can result in differences when comparing trends in the two stages. Soil freezing characteristic curves generally start increasing around -2, so it is intuitive that the warm-cold permafrost distinction captures the increase in
315   H_l trends. However, while the distinction between warm and cold permafrost may be effective at identifying when ground ice *begins* to melt, the breakpoint in T_{za} signals more of a regime shift at which point the warming trends and concomitant H_s trends become significantly diminished, while the changes in H_l also continue to increase.
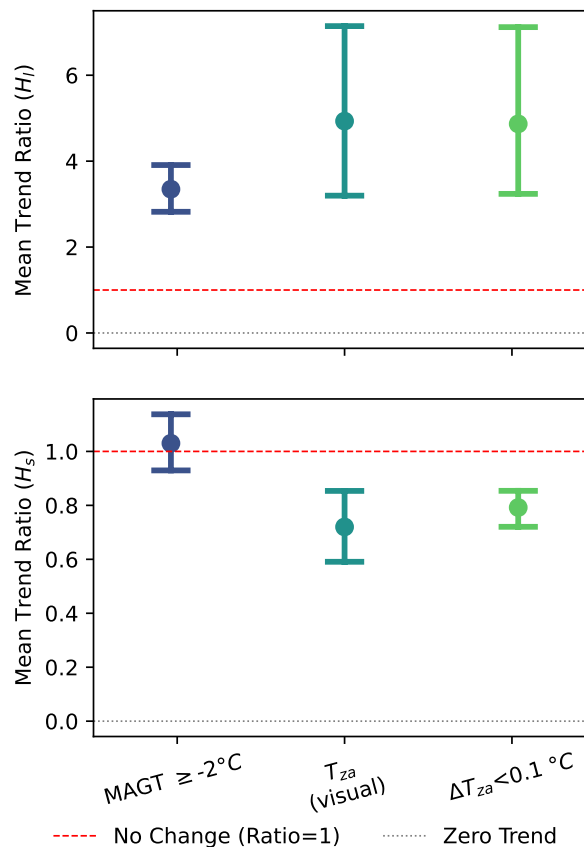
13

Figure 2. The distinction between *warm* and *cold* permafrost (MAGT $\geq -2°C$) distinguishes two distinct stages of H_l trends, but not H_s. However, the breakpoint in T_{za} distinguishes changes in both H_s and H_l trends whether it is identified manually (visual) or quantitatively ($\Delta T_{za} \geq 0.1°C$). Points and bars represent the mean trend ratio (after/before) and the 95% confidence interval, respectively.

4.4 MAGST

In all simulations, trends in MAGST resemble those of total sensible heat. MAGST shows strong interannual variability. In our simulations, MAGST trends are not visibly affected by phase change near 0 °C even when warming at depth decreases significantly. MAGST trends were roughly 0.40 °C dec^{-1}.

At low temperatures, the difference between MAGST and MAGT or T_{za} remains stationary slightly above 0 °C. When the ground warms to near 0 °C, MAGT trends within permafrost with some ice reduce in magnitude, while MAGST trends are unaffected. This period is also accompanied by inflection points in the borehole latent heat trends. Therefore, $MAGST - T_{za}$ can become an additional TSP metric where an increasing trend indicating increased latent heat uptake, while deeper observations remain isothermal at 0 °C.

14

Conceptually, treating MAGST change as a proxy for permafrost change is not entirely appropriate because MAGST is observed in the active layer and changes in permafrost respond with some delay to surface change. However, MAGST may still be useful as an indicator of subsurface heat gain for several reasons: (1) Averaged over longer periods, the impact of lag
330 time is reduced. (2) MAGST is minimally affected by latent heat; in our simulations, even during periods of significant phase change, we do not observe a reduction in MAGST trends. (3) Many thaw phenomena occur closer to the ground surface than to a depth of 10 m and MAGST can give more direct insight into the lateral variation of temperature and temperature trends that may drive those changes than deeper, and much more costly, MAGT. The strong lateral variation of MAGST can be addressed with dedicated sampling (e.g., Gubler et al., 2011; Gruber et al., 2018a; Stewart-Jones et al., 2023).

335 **4.5 Depth of zero annual amplitude d_{za}**

The d_{za} is determined by the surface temperature and the attenuation of the annual temperature wave with depth. The latter property is governed by the thermal diffusivity of the soil column and phase change affecting the apparent thermal diffusivity. We therefore expected that d_{za} would tell us something about increased H_l.

Our simulations show that large increases in d_{za} can occur even when there is relatively little change in H_l and large
340 increases in H_l occur with small changes in d_{za} (Figure 1). However, without change in H_l, we do not observe changes to d_{za}: in all simulations, bedrock profiles—which contain no moisture—exhibit no long term trend in d_{za} regardless of temperature. In these cases, the d_{za} is stationary about some mean value, with fluctuations due to interannual changes in surface amplitude. In icy soil, we found d_{za} to decrease to as little as 3.1 m before deepening in the late-stage warming phase.

We find a temperature-dependent relationship between d_{za} and column heat gain. The exact point at which the sign of d_{za}
345 changes during warming depends on the configuration of climate and ground simulated, but it should be expected when T_{za} is close to 0 °C and when d_{za} is close to ALT. In cold permafrost, d_{za} decreases as permafrost warms because more time is spent at temperatures with phase transition that attenuates the annual temperature wave. At a certain point, a borehole becomes completely isothermal and d_{za} stays relatively constant. Following this, as TOP lowers and ALT increases, the d_{za} becomes shallower, approximating TOP.

350 The relationship between d_{za} and H_l is nonlinear. Instead, the interpretation of d_{za} is more nuanced, and it can provide information about increased liquid water content. Changes to d_{za} reflect changes in the *annual range* of liquid water content, vertically integrated from the surface downward. In warming permafrost, if we assume that the increase in temperature range is the result of a greater maximum annual water content (and not a decrease in the annual minimum), then the annual mean water content will also increase by some amount. Therefore, a trend to a shallower d_{za} does correspond to an increase in H_l
355 even if it does not correspond linearly to *total* column H_l. Another consideration is that the metric only responds to changes above d_{za}; the large increases in latent heat seen in Figure 1h may be due to melting taking place deeper in the profile.

The shallow limit reached by d_{za} in Figure 1i reflects the choice of cutoff used to define *zero amplitude* (0.1 °C in this case) and a smaller cutoff value would result in greater sensitivity to change for shallow d_{za} values because it would take longer to reach the limit. Overall, the relationship of d_{za} to warming is temperature dependent, consistent with Changwei et al. (2015).

15

360   Despite the additional complexity, d_{za} trends can be used to infer changes in H_l and freeze-thaw behaviour. Its behaviour is qualitatively distinct from ground temperature, providing unique insights.

4.6   Annual thermal integral ($\bar{\tau}$)

The mean annual borehole temperature $\bar{\tau}$ over a chosen integration depth exhibits behaviour that is often intermediate between the rapidly fluctuating MAGST and the much steadier MAGT. Qualitatively, $\bar{\tau}$ time series correlate with changes in H_s.

365   During near-isothermal periods, $\bar{\tau}$ often resembles H_s more than MAGT. Although no published $\bar{\tau}$ trends exist, the magnitude of modeled trends can be reasonably compared to MAGT or MAGST trends because $\bar{\tau}$ is normalized to represent an average borehole warming.

The balanced influence of temperature trends over a range of depths makes $\bar{\tau}$ less susceptible than MAGT to producing undetectable trends when boreholes become near-isothermal. This comes at the cost of greater interannual variability because

370   of the incorporation of near-surface temperatures.

4.7   Accelerating thaw rates

In simulations with appreciable ice content, we observe a transition from moderate to accelerated permafrost degradation as the permafrost becomes very warm (e.g., ca. 2060 in Figure 1 g–l). This occurs after the permafrost becomes sufficiently warm, coinciding with the reversal of the d_{za} trend.

375   We interpret the accelerated degradation to be caused primarily by the development of isothermal conditions which limits the re-establishment of a temperature gradient in winter to draw heat out of the ground (Connon et al., 2018). This phenomenon has been discussed in the context of talik formation as a driver of tipping-point behaviour in peatlands and discontinuous permafrost (Connon et al., 2018; Devoie et al., 2019). Because our simulations do not consider water transport out of—and the subsequent drying of—the active layer, any melted ice persists as water; we expect this would accentuate the inhibition of

380   freezing due to latent heat.

4.8   The effect of monitoring depth on warming rates

The differences in 10-year MAGT warming rates between 10 m and 20 m are positively skewed (Figure 3a) with modal values of less than 0.1 °C dec^{-1}. Nevertheless, across all soil types, 50% of observation windows have more than 0.23 °C dec^{-1}, 10% have more than 0.60 °C dec^{-1}, and 5% have more than 0.72 °C dec^{-1}. Very low trend differences are attributed to low

385   warming rates associated with warm, near-isothermal conditions in icy materials.

When trend differences are normalized their distribution becomes less skewed (Figure 3 b) and the effect of ground materials is reduced. 50% of windows have MAGT trend differences greater than 73%, 10% have differences greater than 291% and 5% have differences greater than 555% .
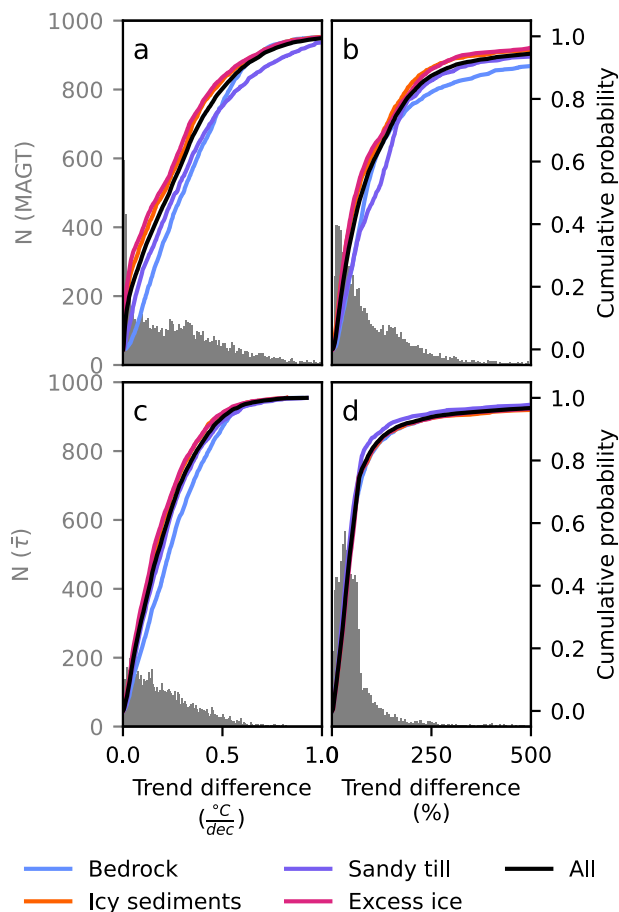
16

Figure 3. The effect on 10-year trend magnitude is greater for MAGT observation depth than for $\bar{\tau}$ total integration depth. This is true for both absolute and normalized differences. Grey histograms show the distribution of differences in 10-year trends for MAGT (a, b) and $\bar{\tau}$ (c, d) between observation or integration depths of 10 and 20 m across all terrain types (left axis). Coloured lines represent differences broken out by terrain type and plotted as cumulative distribution functions (right axis). Subplots (a) and (c) represent absolute differences. Subplots (b) and (d) represent normalized differences.

In $\bar{\tau}$ trends, the impact of different integration depths and the effect of terrain type is weaker than in MAGT trends (Figure 3 c). However, icier locations still exibit reduced differences. Compared to MAGT, the distribution of values is less positively skewed. The variabilities at 50, 90 and 95% probability are 0.17, 0.45, and 0.53 respectively.

When $\bar{\tau}$ trend differences are normalized, there is virtually no difference between different ground types (Figure 3 d). The differences at 50, 90 and 95% probability are 44, 156, and 319%, respectively.

In summary, a difference in observation depth can introduce meaningful differences in the revealed decadal warming trends (Figure 3). It is greater than 0.23 °C dec^{-1} in 50% of our simulated trend windows across all ground types. To contextual-

0.20 ± 0.10 °C dec^{-1} in discontinuous permafrost, based on sensors that are between 5 m and 24.5 m deep. The magnitude and
uncertainty of warming rates presented there are commensurate with the uncertainties due to sensor position we show.

The differences of $\bar{\tau}$ trends caused by integration depth are lower than for MAGT observation depths (Figure 3c,d). Additionally, sites can be more meaningfully compared even when the sensors may not be at the same depth because $\bar{\tau}$ can be interpolated to a common depth where sensors at the same depths are not available.

4.9 Predictiveness statistics for all TSP metrics

For each TSP metric and heat content (H_s, H_l, and H_t), the percentage of significantly positive and significantly negative correlations are recorded across all moving windows in the simulation results. A detailed example for a single metric and heat variable is shown in Figure 4 where most correlations are positive and increases in T_{za} correspond to increasing H_s. However, in as many as 2% of 5-year windows and 4% of 20-year windows, this correlation is negative. Results for all simulations are summarized in Table 3 and the remaining figures are included in the Supplementary Material (S1).

The impact of sensor quality on predictiveness is within a few percentage points for most TSP metrics with a few exceptions. The predictiveness of TOP is decreased with decreased sensor quality (most notably for $\mathcal{Q}_2$) for all heat variables and for all window sizes. The predictiveness of MAGT (T_{10}, T_{15}, and T_{20}) for H_l is also appreciably decreased with decreasing quality for 5-year windows, but not for longer window sizes. Additionally, the impact of sensor quality is greatest for larger observation depths (T_{20}).

Predictiveness for d_{za} is low overall, but when observation windows are split into *warm* and *cold* scenarios according whether t_{za} is above or below -0.5 °C, the percentage of significant windows increases. For cold permafrost, d_{za} achieves predictiveness values up to 75% for H_l in 20-year windows. In warm periods, d_{za} achieves predictiveness values up to 75% for H_l in 20-year windows. When averaged over all time windows and levels of sensor quality, metrics describing annual temperature averages (MAGT and $\bar{\tau}$) rank among the highest for both H_l and H_s.

Without exception, the predictiveness of the metrics decreases for shorter temporal windows. Most metrics have scores of less than 30% for 5-year windows. However, TOP-H_l is the exception, with a score as high of 57%. For short windows, $\bar{\tau}$ is a more consistent proxy for H_s and H_l than single-depth temperature measurements, these also score more than 50% in 5-year windows.

The predictiveness of most metrics is larger for H_s than for H_l. However, TOP-H_l is the exception, predicting H_l better. Values for H_t are not simply weighted averages of H_l and H_s: the predictiveness of H_t is consistently greater than either H_l or H_s for T_{10}, T_{15}, T_{za}; smaller for MAGST; and intermediate between the two for $\bar{\tau}_{10}^0$, $\bar{\tau}_{15}^0$, and $\bar{\tau}_{20}^0$. For d_{za}, H_t is intermediate for 10- and 20-year windows, and greater for 5-year windows.

We interpret a larger number of significant values to indicate that an increase in a given metric more reliably indicates an increase in the heat variable of interest over a randomly selected observation window. However, the time- and location-dependent relation between the metric and heat content means that we do not interpret these results in terms of the *strength* of the relation. Also, because we only simulate a warming trend, we generally interpret *reversed* correlations as a consequence of
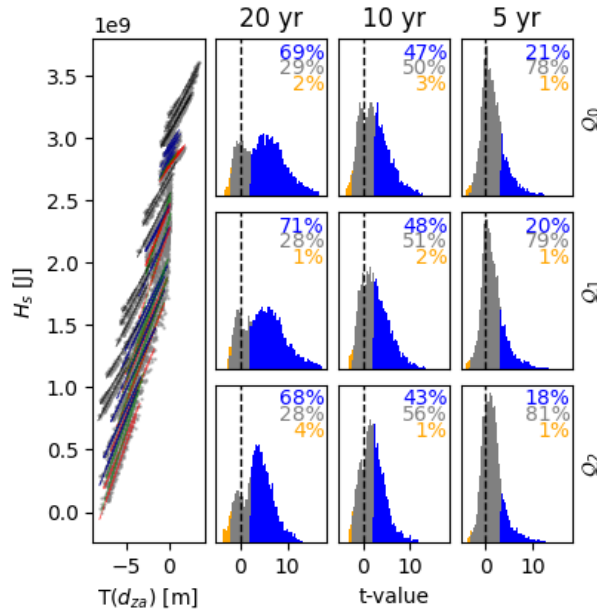
Figure 4. Effect of sensor quality and data length on the significance of metric (Tza) - heat (H_s) relationship. Larger t-values indicate a more reliable relationship between changes in metric and changes in heat content. More consistently positive or negative t-values demonstrate a less ambiguous interpretation from the metric. In this example, Left panel shows correlation over each complete simulation; data points represent annual metrics. Regression lines are coloured according to ground material: bedrock (black), sandy till (green), icy sediments (red), excess ice (blue). Each histogram shows the distribution of test statistics for different averaging windows (5, 10, and 20 years) and noise levels (0, 50, and 100 mK). Each distribution is colour coded according to whether the regression within the window is significantly negative (orange), significantly positive (blue) or not significant (grey). Significance is assessed at p < 0.05. These percentages are included as text at the upper right corner of each panel.

430   one of three factors: interannual variability, temporal window mismatches due to time lags, and errors due to decreased sensor quality. For example, the negative correlations in Figure 4 would not be caused by an increase in the metric when H_s decreases within the window, but rather by a decrease in the metric (for one of the three reasons stated above) as the H_s increases.

In general, we see that our sensor imperfection model results in only a small effect on the effectiveness of metrics as predictors, except for short observation periods. For MAGT, we expect the effect of normally distributed noise is likely erased

435   in individual sensor records because they are averaged over the year. We expect the bias and trend in $\mathcal{Q}_2$ also contributed to the lower performance.

Averaging multiple sensors in the calculation of $\bar{\tau}$ would also reduce the impact on the metric of sensor drift and bias in any individual sensor. On the other hand, the calculation of annual maxima required to estimate TOP relies on single data points and involves no averaging—this would be directly affected by sensor bias and noise. This would therefore more strongly

440   affect metric performance by amplifying, rather than dampening, the effect of deviations from the perfect model data. d_{za}

Table 3. Test statistics measuring how reliably each metric corresponds to the sensible, latent, or total ground heat content for a given averaging window and data quality. Numeric values represent the percentage of significantly positive (left) or negative (right) relationships across all observation windows (corresponding to the blue and orange percentages in e.g., Figure 4). A colourized version is available in the supplementary material.

	Window	20 years			10 years			5 years			20 years			10 years			5 years		
	Dataset	Q_0	Q_1	Q_2	Q_0	Q_1	Q_2	Q_0	Q_1	Q_2	Q_0	Q_1	Q_2	Q_0	Q_1	Q_2	Q_0	Q_1	Q_2
H_l	$MAGST$	72	71	71	49	49	49	22	22	22	0	0	0	0	0	0	0	0	0
	T_{10}	93	92	90	64	62	57	28	26	18	0	0	0	0	0	0	0	0	0
	T_{15}	85	85	83	52	52	48	32	32	24	0	0	0	0	0	0	0	0	0
	T_{20}	73	75	48	47	47	23	32	32	9	0	0	22	0	0	19	1	2	8
	$\bar{\tau}_{10}^0$	88	88	88	57	57	56	27	27	27	0	0	0	0	0	0	0	0	0
	$\bar{\tau}_{15}^0$	90	90	90	57	57	57	26	26	26	0	0	0	0	0	0	0	0	0
	$\bar{\tau}_{20}^0$	90	90	90	57	57	56	26	26	25	0	0	0	0	0	0	0	0	0
	$d_{za}(warm)$	10	10	10	5	5	6	2	2	3	48	48	47	20	21	19	10	10	9
	d_{za}	44	44	44	32	32	32	14	14	14	22	22	24	9	9	10	4	4	4
	$d_{za}(cold)$	74	75	71	57	57	54	26	25	23	0	0	0	0	0	1	0	0	0
	T_{za}	59	59	55	32	34	26	14	14	11	0	0	4	1	0	2	1	1	1
	TOP	96	97	86	90	91	68	57	55	38	0	0	0	0	0	0	0	0	0
H_s	$MAGST$	75	75	75	54	54	54	22	22	22	0	0	0	0	0	0	0	0	0
	T_{10}	91	91	92	72	75	78	48	50	54	0	0	0	0	0	0	0	0	0
	T_{15}	92	93	92	64	64	67	28	27	28	0	0	0	0	0	0	0	0	0
	T_{20}	90	92	70	54	55	44	17	17	13	0	0	16	0	0	4	0	0	1
	$\bar{\tau}_{10}^0$	96	96	95	81	81	80	66	66	65	0	0	0	0	0	0	0	0	0
	$\bar{\tau}_{15}^0$	98	98	98	85	85	85	71	71	71	0	0	0	0	0	0	0	0	0
	$\bar{\tau}_{20}^0$	99	99	99	89	89	88	74	74	74	0	0	0	0	0	0	0	0	0
	$d_{za}(warm)$	2	2	2	3	3	4	2	2	2	62	62	55	25	24	19	7	7	5
	d_{za}	29	29	30	24	24	25	16	15	16	26	26	24	10	10	8	2	2	2
	$d_{za}(cold)$	48	48	48	41	41	39	26	26	25	0	0	0	0	0	0	0	0	0
	T_{za}	68	70	68	47	47	42	20	20	18	2	1	4	2	1	1	1	0	0
	TOP	78	78	64	39	38	34	18	17	16	0	0	0	0	0	0	0	0	0
H_t	$MAGST$	65	65	65	41	41	40	17	17	17	0	0	0	0	0	0	0	0	0
	T_{10}	97	98	96	86	86	86	51	51	50	0	0	0	0	0	0	0	0	0
	T_{15}	98	98	96	78	78	77	34	34	29	0	0	0	0	0	0	0	0	0
	T_{20}	93	95	71	67	68	43	27	27	11	0	0	18	0	0	16	0	0	4
	$\bar{\tau}_{10}^0$	94	94	93	69	69	68	50	50	50	0	0	0	0	0	0	0	0	0
	$\bar{\tau}_{15}^0$	97	97	97	75	75	75	55	55	55	0	0	0	0	0	0	0	0	0
	$\bar{\tau}_{20}^0$	98	98	98	79	79	78	58	58	58	0	0	0	0	0	0	0	0	0
	$d_{za}(warm)$	2	2	3	4	4	4	2	2	3	50	50	47	21	21	20	10	10	9
	d_{za}	34	34	34	29	29	29	18	18	18	20	20	21	9	9	9	4	4	3
	$d_{za}(cold)$	56	56	54	47	48	47	29	29	28	0	0	0	0	0	0	0	0	0
	T_{za}	77	77	71	51	52	45	22	22	18	0	0	3	0	0	1	0	0	1
	TOP	87	88	71	61	62	45	33	32	20	0	0	0	0	0	0	0	0	0

also requires additional calculations, but the performance of this metric is not similarly affected; the method by which it is calculated also averages amplitude data from multiple sensors.

The large impact of decreased sensor quality on T_{20} which shifts the results towards a negative correlation may illustrate a weakness of the methodology which is that we only perform a single realization of the randomized sensor quality model. In

445   this case, it may be that the realization produced significantly more negative trends at that depth. Alternatively, it is possible that the sensor bias and drift have a larger effect because the signal magnitude is much smaller at that depth.

d_{za} shows a different signal in warming boreholes than other metrics (Figure 1 c,i). However, the predictiveness is low, and possibly unuseably so for short observation windows (Table 3). We attribute this to both the noisy nature of the metric and the period of stagnation prior to the reversal of the trend. We interpret the lower predictiveness of d_{za} as a consequence of both

450   the noisier signal and the temperature-dependence of the metric. The higher interannual variability means that longer temporal windows are needed to obtain clear trends. More importantly, the results highlight the importance of defining a precise cutoff at which the behaviour of d_{za} reverses.

$\bar{\tau}$ is a more reliable indicator of H_s and H_t change over shorter observation periods than MAGT (e.g $T_{20}, T_{15}, \ldots$). This is in spite of the greater interannual variability of $\bar{\tau}$ caused by the inclusion of near-surface measurements. Intuitively, we

455   expected this variability to make trends harder to predict. We believe that this effect is outweighed by the diminished impact of latent heat in warm conditions, which causes MAGT trends to become greatly diminished. It is also interesting to note that although qualitatively $\bar{\tau}$ behaves similarly to a superimposition of MAGST and MAGT, both of those metrics are more strongly affected by shorter observation windows. We interpret this to mean $\bar{\tau}$ benefits from being depth-integrated, which more closely resembles how H_s would be calculated if heat capacities were known.

460   **4.10   Summary of insights from testing TSP metrics with simulation experiments**

MAGT is traditionally the most widely used metric to report permafrost change. It is a direct measurement of the permafrost and it reveals how quickly the permafrost thermal state is changing at a specific depth. Trends correlate well with column heat contents, but the relationship is time-, depth-, and location-dependent. As a consequence, comparing (between locations or times) and aggregating MAGT trends usually involves blending dissimilar physical processes, producing a number with no

465   meaningful connection to either heat gain or ice loss. Therefore, MAGT trends are most useful for detecting the presence and sign of a trend. The metric is also prone to periods of imperceptible change, making quantification difficult.

$\bar{\tau}$ is a good indicator of changes in borehole sensible heat (H_s), already over shorter time periods, outperforming MAGT in this regard. It is less prone to stagnant behaviour, making trend detection more reliable. It also takes advantage of all available sensors. Practically, it allows for compensation of unequal monitoring depths through standardized integration, improving

470   comparability between boreholes. While being subject to the same limitations as MAGT in principle, the confounding effects of latent heat on the ability to compare or aggregate trends are reduced for $\bar{\tau}$.

Despite the common definition of MAGT as the temperature at d_{za}, we find little support for using T_{za} as a TSP metric to monitor permafrost change. In addition to the greater complexity of calculating this metric, it is the first one to become isothermal in the simulations as the ground warms. It is also less predictive of column heat content compared to MAGT or

475   $\bar{\tau}$ (Figure 3). However, it may be useful for (1) indicating near-isothermal behaviour in a borehole because it will be the first metric to achieve this, and (2) as a classifier for late-stage permafrost thaw; in our simulations, the point at which T_{za} reached approximately 0 °C coincided with the transition in sign of the d_{za}-warming relation.

TOP is a straightforward metric for temperature-based monitoring with a clear physical meaning, describing changes in permafrost thickness. It behaves similarly to ALT or $\bar{\mathcal{D}}$ but with some clear advantages. The definition of TOP is purely thermal

480   and less ambiguous than that of ALT, which is alternatively defined based on temperature or phase state (van Everdingen, 1998; Burn, 1998). Additionally, the direction of ALT trends reverses after the formation of a supra-permafrost talik while TOP remains monotonic. Although $\bar{\mathcal{D}}$ may have inherent meaning, it is qualitatively similar enough to TOP that there is little to gain by including both in a parsimonious set of metrics. Adopting TOP as a primary metric also does not diminish the utility of existing ALT records and monitoring programs; in the absence of a talik, TOP can be considered equivalent to the purely

485   thermally defined ALT.

Overall, TOP is a good proxy for H_l even in short time windows, even though the exact correspondence is unknown without quantification of ice content. In our simulations, it increases slowly in the early stages of warming and then accelerates in later stages of warming. TOP has an easily understood physical meaning, describing a change directly affecting permafrost thickness. However, the accuracy with which it can be estimated is more strongly affected by sensor spacing (e.g., Riseborough,

490   2008) and quality than other metrics. Some confounding may originate from subsidence caused by a rising permafrost base.

d_{za} can be used to infer changes to H_l, but it provides an incomplete picture: phase change below d_{za} is invisible, the upper limit of d_{za} is affected by the choice of cutoff for 'zero amplitude', and the sign of the correlation between d_{za} and H_l is temperature-dependent. However, the behaviour of the metric is qualitatively distinct from ground temperature, which can be helpful in interpreting permafrost changes.

495   Given the above results, we recommend TOP, d_{za}, and $\bar{\tau}$ in addition to MAGT as a parsimonious set of metrics for quantifying permafrost change. MAGST can be considered as an additional metric that, while not observed in permafrost, provides the clearest measure of how climate or disturbance drive changes at depth.

5   Case study with observations from GTN-P

As a demonstrator with field observations, we calculated TSP metrics for selected ground temperature records from the GTN-P

500   database. Data were downloaded for all boreholes with available temperature time series. 38 sites met our initial criteria: (1) at least 5 years of data; (2) at least daily measurement frequency; (3) a maximum observation depth of at least 5 m; and (4) at least 5 depths of observation. After manual removal of datasets with excessive noise or data gaps, 14 boreholes from 10 areas were retained; 9 areas were located within the European Alps, and one within Russia. Three boreholes—Samoylov, Ritgraben (RIT_0102) and Schilthorn (SCH_5198)—have been selected for this demonstration and GTN-P data was supplemented with

505   more recent observations from PERMOS (Swiss Permafrost Monitoring Network, 2024) for the two Swiss sites.

The three sites illustrate the utility of using multiple TSP metrics for revealing change (Figure 5), especially in warm permafrost. Samoylov, located in Russia, is in the Lena River Delta within the continuous permafrost zone. The observed
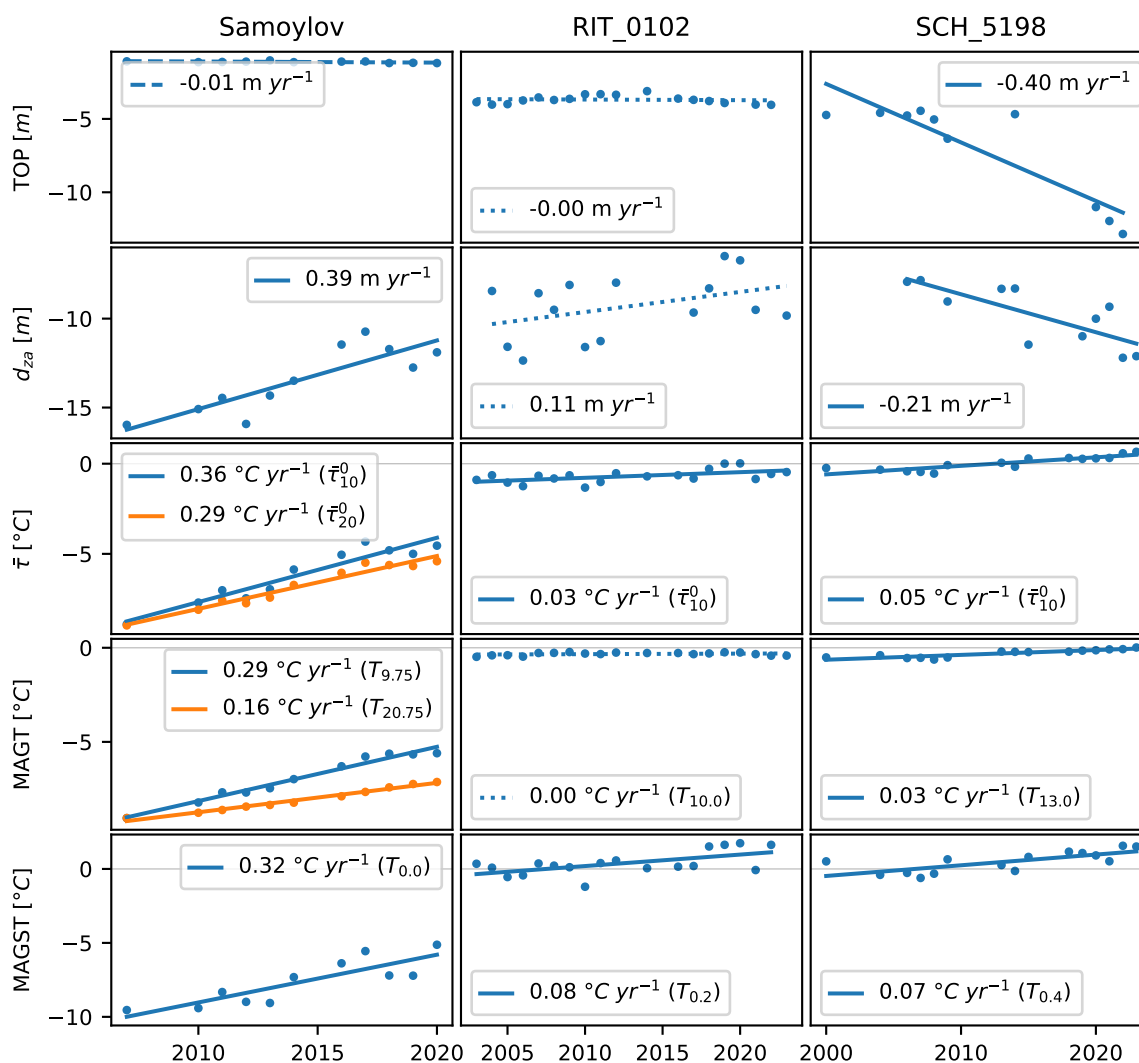
Figure 5. Selected TSP metrics calculated for three GTN-P monitoring boreholes. Solid trend lines are significant at p<0.05, dashed trend lines are significant at p<0.1, and dotted trend lines have p≥0.1. Where appropriate, depth information is included in each figure legend.

warming rates of 2.9 °C dec^{-1} at 9.75 m and 1.6 °C dec^{-1} at 20.75 m are high, consistent with cold permafrost. The difference in warming rates between the two observation depths is also high at 1.1 °C dec^{-1} (a 54% difference). In contrast, the other two 510 sites are located in Switzerland, in warmer permafrost. Warming rates at these locations are much lower. At RIT there is no detectable warming trend at 10 m and at SCH the warming rate is 0.3 °C dec^{-1} at 13.0 m: typically low for warm permafrost.

The MAGST trend at Samoylov is consistent with warming at depth and has a similar magnitude. In contrast, MAGST warming rates at the warmer sites are markedly higher than the MAGT rates. The greater difference between warming at the surface and warming at depth is another indication that latent heat at depth reduces the observed MAGT change. Surface

515 warming rates at all sites are high relative to published values of (e.g., ca. 0.2–0.6 °C dec^{-1} Hu et al., 2019; Wu et al., 2012; Swiss Permafrost Monitoring Network, 2024)

While there are no published $\bar{\tau}$ observations with which to compare these trends, they can be meaningfully compared to either MAGST or MAGT trends. $\bar{\tau}$ increases at Samoylov at a rate between 2.9 °C dec^{-1} (20 m integration depth) to 3.6 °C dec^{-1} (10 m integration depth). At two warmer sites, $\bar{\tau}_{10}^{0}$ increases relatively slowly: by 0.3 °C dec^{-1} at RIT and by 0.5 °C dec^{-1} at

520 SCH.

At RIT, estimated TOP change rates (0 cm yr^{-1}) do not provide any indication of change. At Samoylov, a change rate of -1 cm yr^{-1} is modest relative to observations elsewhere (e.g., Smith et al., 2022) and low when compared to the degree of thermal change taking place. However, at SCH we observe rates of -40 cm yr^{-1} which is among the highest observed rates globally. This also is in contrast to the modest warming signals seen at the site.

525 At each site, we observed changes to d_{za} during the observation period. At Samoylov and RIT, d_{za} is becoming shallower, consistent with the first phase of warming and indicative of greater freeze-thaw activity and increased transfer of latent heat in the soil column. d_{za} change is slightly greater at Samoylov (+3.9 m dec^{-1}) compared to the warmer RIT (+1.1 m dec^{-1}). At SCH, the magnitude of d_{za} change is greatest (-2.1 m dec^{-1}) and its direction has changed, consistent with late-stage warming found in our simulations.

530 The use of multiple TSP metrics allows us to quantify and qualify permafrost change. We can group the metrics into 3 categories: temperature (MAGT, MAGST, $\bar{\tau}$), vertical extent (ALT, TOP), and phase change (d_{za}). With a multi-metric approach, different aspects of change can be revealed.

At Samoylov, three out of three temperature-based metrics indicate rapid warming, and d_{za} indicates increased involvement of latent heat in the ground thermal regime but there is no TOP change. Change is occurring in 2 categories.

535 At RIT, one temperature-based metric (MAGT) indicates no change and two show some change is taking place. In addition, there is no TOP trend over the observation period. Taken in isolation, these data suggest little change is taking place. With some interpretation, such as the near-zero MAGT and borehole location, we are able to add an additional qualitative interpretation that change rates are suppressed due to latent heat. Finally, with calculated d_{za} change rates, we can quantify one dimension of change that can be compared to other locations.

540 At SCH, two out of three temperature-based metrics indicate slight warming and one indicates moderate warming. TOP is changing rapidly. The deepening d_{za} shows that the site is in a late stage of warming and permafrost degradation.

6 Discussion

6.1 Testing TSP metrics with simulated data

Simulations represent an ideal scenario with which to evaluate the metrics but they can only provide some of the complexity

545 of the real environmental system. In practice, heterogeneous subsurface characteristics will mean observations at an individual depth are less well representative of permafrost above and below. Spatially variable ice content will amplify or dampen the response of these metrics to thaw, and this will affect rates of change. Instrumentation density has a major impact on the

accuracy and precision of many metrics (e.g., Hinkel, 1997) and will affect the resolution with which some of the metrics can be calculated.

550   Another consideration is the consequence of moisture transport. In our simulations, there is no water flow within or out of the simulation with the exception of melted excess ice. This means that during late-stage thaw in warm, icy simulations with a supra-permafrost talik, the d_{za} becomes shallower than the top of permafrost, and is kept shallow by the buffering effect caused by freeze-thaw cycles of supra-permafrost water. It is plausible that an overall loss of moisture above the permafrost table during this period could prevent the d_{za} from ever reaching the top of permafrost, or alternatively accelerate the late-stage

555   shallowing of d_{za}.

In addition to using these metrics for interpretation of borehole change, they can also be used to provide further information for models that do not output variables such as column heat contents or isotherm locations.

Representing change as a single per-borehole statistic is challenging because of differences in data completeness and measurement density in boreholes. Observational records in boreholes differ in their vertical extent and duration. Averages can

560   therefore mask locations with strong change when boreholes are very deep or have many sensors or exaggerate measures of change in boreholes with few sensors.

6.2   Interpretability of MAGT trends

Our results show that increasing MAGT is consistently indicative of increases in column H_l and H_s even in the presence of distortion from sensor noise, bias, and trends. However, the exact quantitative relationship is location- and time-dependent. In

565   this regard, it may be the direction of the trend from which meaning can be most unambiguously derived. However, given that the vast majority of permafrost boreholes are warming (Biskaborn et al., 2019), this may be an almost trivial conclusion.

Our results suggest that MAGT can contribute to a descriptive picture of permafrost change, but only when used in combination with other temperature-derived metrics. In isolation, the magnitude of MAGT trends can be attributable to both the effect of latent heat and the intensity of surface warming. With a more complete suite of indicators, the effect of latent heat can

570   be made more explicit and permafrost change can be quantified more reliably.

Our results highlight the challenges of comparing trends between boreholes or regions. In our simulations, the behaviour of each metric generally follows a similar trajectory. For MAGT, this is: rapid warming, reduced warming, no warming, and finally rapid warming if thaw progresses to the observation depth. Most importantly, we do not change the magnitude of the warming trend at the surface, yet the trends measuring permafrost response show a great deal of variability across simulations and at

575   different points in time. Therefore, in our experiments, MAGT tells us more about the configuration of the system and the *stage* of thaw than about the intensity of the warming trend. In this regard, the resolution of MAGT as a *climate* indicator may indeed be limited to the trend direction discussed above. In reality, locations will be subject to different trends in air temperature, snowpack and vegetation; all of which will affect warming rates at depth. However, this signal will be superimposed on the purely permafrost-dependent variability which, as we have shown, is on the same order of magnitude as observed trends.

580   Our results also provide some guidance on how to make MAGT trends more interpretable. If we are interested in understanding where permafrost change is happening faster or more slowly, groupings should account for both the ground conditions and

some other indicator of the *stage* of warming. We show that T_{za} is a good candidate for this. The breakpoint in the T_{za} trend is able to separate warming into two stages with statistically distinct trends in H_s and H_l. The performance of the T_{za} breakpoint is superior to the traditional classification of warm permafrost (MAGT > -2 °C) which does not discriminate H_s trends in the two stages. This is significant because H_s trends are strongly linked to temperature. This approach also has the advantage that T_{za} often requires only relatively shallow observations because d_{za} becomes shallower as the borehole warms.

Current comparisons and aggregations of MAGT trends are most commonly grouped by region or permafrost zone. This partially accounts for temperature and warming stage, but this is hampered by uneven and biased spatial sampling, particularly in the discontinuous permafrost zone where permafrost temperature may still be strongly affected by surface conditions. In these cases, more meaningful comparisons could be made by further subdividing datasets according to the ground conditions on a spectrum of ice content. However, such fine-scale subdivision may be limited by general lack of ground temperature data and result in too few boreholes in each category to meaningfully compare.

6.3 Permafrost metrics as a climate indicator

Despite its application as a climate indicator, permafrost temperature change is complicated by the effects of latent heat and we should expect permafrost warming rates to diminish as boreholes approach 0 °C. One possible solution is to consider using only boreholes with very little ice content, as would be expected in certain kinds of bedrock. Such an approach has been suggested by Smith and Riseborough (1996), who recommend monitoring in exposed bedrock to obtain the most direct climate signal from ground temperatures. Notably, bedrock sites are underrepresented in much of the permafrost monitoring data because of difficult drilling conditions, and because permafrost impacts are often caused by thaw of ice-rich ground.

6.4 Temperature-dependence of d_{za} trends

Changwei et al. (2015) also show observations of reversing d_{za} behaviour and explain this behaviour with an equilibrium model (i.e., analytic heat conduction equation with a sinusoidal surface temperature variation). However, a limitation of this approach is that the transition in correlation sign cannot be examined—their warm, deep-d_{za} simulation only exists as a fully thawed profile rather than one with dynamic behaviour. Our transient simulations show that this reversal can take place over several years during which the d_{za} changes very little and the sign of the correlation between d_{za} and air temperature is undefined.

This distinction is important because other studies report unidirectional (and conflicting) relationships between warming trends and d_{za} (e.g. Bonnaventure et al., 2015; Wang et al., 2022). An important next step in this approach to monitoring will be developing additional criteria to more clearly delineate when a positive- or negative- correlation should be assumed.

6.5 Accelerated permafrost degradation and implications for monitoring

We observe accelerated degradation (lowering of TOP) in warm permafrost as it becomes isothermal and develops a supra-permafrost talik. Similar discrepancies have been described elsewhere. On the Tibetan Plateau, ALT deepening rates have been shown to be greater in warm permafrost than in cold permafrost (Changwei et al., 2015). In discontinuous permafrost and

peatlands, taliks have been described as giving rise to tipping-point behaviour and kicking off rapid degradation (e.g., Connon et al., 2018; Devoie et al., 2019). We observe this phenomena across different stratigraphic types (Table B1) and climates,

615 representing a wide range of permafrost conditions. This pattern suggests a greater abundance of this tipping point behaviour than may have previously been considered.

Such rapid change could affect permafrost monitoring efforts by causing TOP to descend rapidly out of the measurement range of existing thaw tube installations (O'Neill et al., 2023). This is also another example of how the magnitude of trend rates for TSP metrics are more indicative of local conditions than of climatic forcing.

620 Certain TSP metrics may offer insight as to when this accelerated degradation may occur. In our simulations, it is preceded by the breakpoint in T_{za} and the halting of the d_{za} shallowing trend. These can act as quantifiable indicators that permafrost is in late-stage thaw and that subsequent talik formation and rapid degradation are imminent.

7 Conclusions and recommendations

We investigated the long-term behaviour of a suite of temperature-derived metrics as indicators of permafrost thaw.

625 Our results suggest that calculating multiple temperature-derived TSP metrics provides rich information for characterizing and understanding permafrost change, particularly in warm permafrost. In addition to MAGT, we recommend TOP, d_{za}, $\bar{\tau}$, and MAGST as a parsimonious set of five metrics. The suitability of individual metrics as indicators of change varies through time in the simulations. While most experience periods of time with no change—even as borehole latent and sensible heat contents increase—the exact timing of these periods differs between metrics.

630 We find that a multi-metric approach to change monitoring makes it possible to identify and quantify change in isothermal boreholes during periods where MAGT and even ALT trends may be negligible. For example, in a sample of observational data from the GTN-P database we observe strong d_{za} trends in boreholes. These trends can exhibit a distinctly different signal than either MAGT or ALT.

The impact of monitoring depth on MAGT trends is commensurate with both the magnitude and uncertainty of warming rates

635 reported elsewhere (e.g., Biskaborn et al., 2019; Smith et al., 2022). This effect exceeds 73% of trend values and is strongest in soil with little moisture content. This demonstrates the difficulty of interpreting permafrost warming trends in general and should be taken into consideration when calculating uncertainty bounds for averages for zonal permafrost warming. Borehole-averaged warming rates (thermal integrals) alleviate the challenge of comparability somewhat by averaging to a common column depth. However, differences in the total integration depth still produce commensurate differences in observed rates of

640 change.

Caution is advised when interpreting change in permafrost as a climate indicator because of the time- and material-dependent response of many of the metrics to warming; wide variability in observed trends is possible even in the absence of differing climate signals. Most metrics can be used as an indicator of warming vs. cooling but even the sign of the climate-metric relationship can change over time, as we show with d_{za} and ALT. For MAGT, $\bar{\tau}$, and d_{za}, quantitative comparison and aggregation

645 of trends from multiple locations or multiple times (acceleration and deceleration of change) likely produces results with no meaningful connection to heat gain or ice loss.

The relative lack of availability of ground temperature observations with sufficient duration, quality, and measurement frequency to calculate these metrics points to a continued need to support the publication of permafrost data. Furthermore, the long-term view afforded by our simulations can support considerations of improved instrumentation for permafrost monitoring.

650 For example, separate and movable thermistor chains with dense spacing near the permafrost table may help capture changes in TOP, and records of subsidence (Gruber, 2020) may inform estimates of excess ice loss. Similarly, methods of observing and reporting ALT may benefit from adjustments to remain relevant even with talik formation.

Code availability. Newly developed code for calculating metrics is available as a Python package on PyPi (tspmetrics) and at gitlab.com/permafrostnet/tspmetrics. We also use the TSP package which is available at gitlab.com/permafrostnet/teaspoon (Brown, 2022)

655 **Appendix A: Symbolic notation**

T	temperature	°C
t	time	days
z	depth	m
d_{za}	depth of zero annual amplitude	m
T_{za}	temperature at d_{za}	°C
TDD	thawing degree days	°C day
FDD	freezing degree days	°C day
$\bar{\tau}$	thermal integral	°C
$\bar{\mathcal{D}}$	annual thaw-depth duration	$m^3 m^{-2}$
λ_s	thermal conductivity of soil particles	$W m^{-1} {}^{\circ} K^{-1}$
c_s	specific heat capacity of soil particles	$J m^{-3}$
$\mathcal{H}$	heat transfer coefficient	$W m^{-2} K^{-1}$
θ_{sat}	Van Genuchten saturated water content	$m^3 m^{-3}$
θ_{res}	Van Genuchten residual water content	$m^3 m^{-3}$
α	Van Genuchten parameter	m^{-1}
n	Van Genuchten parameter	-
ϵ	Excess ice content	$m^3 m^{-3}$

Appendix B: Model setup and validation

We use the model FreeThawXice1D (Tubini and Gruber, 2025; Tubini et al., 2021) to simulate ground conditions. This model version represents the effects of ground subsidence caused by ice loss within the ground and accurately tracks zero-degree

660 isotherms via local mesh refinement.

B1   Model input and initial conditions

The model is driven by meteorological forcing data obtained using GlobSim (Cao et al., 2019). This tool streamlines the download of reanalysis data, interpolates grid cells to point-scale to make data suitable for 1D simulation, standardizes units and timesteps, and performs heuristic downscaling to account for terrain and other local effects.

Table B1. Stratigraphy definition for four simulation locations.

Stratigraphy	depth [m]	c_s [$\frac{\mathrm{J}}{\mathrm{m}^3}$]	λ_s [$\frac{\mathrm{W}}{\mathrm{mK}}$]	θ_s [$\frac{\mathrm{m}^3}{\mathrm{m}^3}$]	θ_r [$\frac{\mathrm{m}^3}{\mathrm{m}^3}$]	n [-]	α [$\frac{1}{\mathrm{m}}$]	ϵ [$\frac{\mathrm{m}^3}{\mathrm{m}^3}$]
Rock	0–150	890	3.8	-	-	-	-	0
Sandy till	0–1	1920	0.25	0.15	0.05	1	1.7	0
	1–40	1011	1.6	0.35	0.05	0.65	1.67	0.2
	40–150	890	3.8	0.015	0.005	4.06	2.03	0
Icy sediments	0–20	890	3.8	0.015	0.005	4.06	2.03	0
	20–150	890	3.8	0.015	0.005	4.06	2.03	0
Excess ice	0–1	1920	0.25	0.15	0.05	1	1.7	0
	1–60	1011	1.6	0.35	0.05	0.65	1.67	0.2
	60–150	1011	1.6	0.35	0.05	0.65	1.67	0
Heterogeneous excess ice	0–1	1920	0.25	0.15	0.05	1	1.7	0
	1–1.75	1011	1.6	0.35	0.05	0.65	1.67	0.05
	1.75–2	1011	1.6	0.35	0.05	0.65	1.67	0.8
	2–60	1011	1.6	0.35	0.05	0.65	1.67	...*
	60–150	1011	1.6	0.35	0.05	0.65	1.67	0

Values chosen based on (Dall'Amico et al., 2011; Tubini et al., 2021)

*: Alternating values of 0.05 and 0.8 are repeated using the same distribution as the second and third layers

665   We use data from the ERA5 reanalysis to create three sets of meteorological forcing data (1980–2022). One is for Yellowknife, Canada (62.45°N, 114.4°W), one is for a area near Lac de Gras, Canada (64.7°N, 110.4°W), and the last one is for Tombstone Territorial Park in Yukon, Canada (64.56°N, 138.43°W).

    For model spin-up, we repeat the first three years of input data. First, the model is run for 300 years with a 40 m total depth. Next, the deep temperature is extrapolated to 150 m using the geothermal heat flux. The remaining model runs use the 150 m
670 total depth.

    Future conditions are simulated by repeating the last 5 years of input data and changing values using climate projections from Climatedata.ca (Cannon et al., 2015) based on the SSP5-8.5 scenario. We calculate the change in projected annual mean temperature for an arbitrary year relative to the final year of reanalysis data and add this difference to the corresponding year of input data. To simulate different ground conditions, we create five distinct stratigraphies (Table B1).

675 **B2   Atmosphere-ground coupling**

The effects of surface conditions and surface cover such as vegetation and snow are represented with the heat-transfer coefficient $\mathcal{H}$ [$\mathrm{Wm}^{-2}\mathrm{K}^{-1}$]; for a medium of finite thickness such as a snow pack, $\mathcal{H}$ would be derived as a thermal transmittance. In
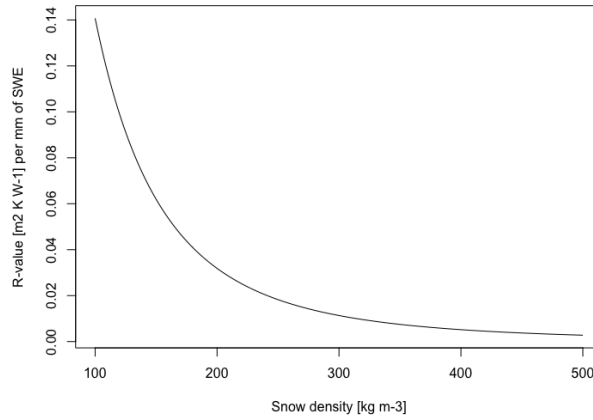
Figure B1. R-value of a snow layer with 1 mm water equivalent, computed with a relationship of snow density and effective conductivity (Fourteau et al., 2021, Eq. 18 for 263K).

equilibrium, it is the inverse of thermal resistance and with oscillating temperature conditions, it may be reduced due to temporary storage and release of heat by the medium characterised (Tubini and Gruber, 2025). During summer, we use a constant

680 value, $\mathcal{H}_s$ and during winter, it is parameterized as a function of the daily snow water equivalent $\mathcal{H}_w$.

Snow-water equivalent (SWE [m]) is computed from daily accumulation and ablation. Snow is accumulated at the rate of daily precipitation for days with a mean air temperature below a threshold of 2.8 °C (e.g., Kienzle, 2008). Snow melts based on a degree-day model (e.g., Rango and Martinec, 1995) whereby SWE is lost at a rate of 3 mm $\text{K}^{-1}\text{day}^{-1}$ when mean daily air temperature is above 0 °C.

685 Snow thermal transmittance is computed from SWE, a proportionality coefficient γ [$\text{Wm}^{-3}\text{K}^{-1}$] translating SWE into an R-value, and an aging function β [days] reflecting densification over time t [days]. To ensure $\mathcal{H}_w$ does not become large without bound as the snowpack thins, we also impose a maximum value ($\mathcal{H}_{max}$) which is also used for snow-free conditions:

$$\mathcal{H}_w(SWE) = max(\frac{1}{(SWE)\,\gamma\,(1-\frac{t}{\beta})}, \mathcal{H}_{max}). \tag{B1}$$

The coefficient γ has a physical basis for individual snow layers (Fig. B1) and is extended here as a parameter characterizing

690 an entire snow pack. In representing for example, taiga and tundra snow packs, γ will parameterize typical conditions such as density and the effect of layering.

B3 Model calibration

To calibrate the simplified snowpack model, we compare model results to ground temperature observations and adjust parameters to ensure that the results are plausible. We use observational data from borehole NGO-DD-2015, a study site in the Northwest Territories located at (64.703 °N, 110.440 °W) (Gruber et al., 2018b, c).

B4 Simulation

Using the input data described above, the model is spun-up from an initial temperature of -3 °C using repeated data (1980–1982), then run until 2100. For the purpose of evaluation, we use output for the period 2016–2021 at which time observations are available. For testing the thaw metrics, we use output for the period 1980–2100.

A set of simulated temperatures are recorded at depths corresponding to the recommended sensor spacing from the PACE Project (Harris et al., 2009) up to a depth of 15 m (i.e., at 0.2, 0.4, 0.8, 1.2, 1.6, 2, 2.5, 3, 3.5, 4, 5, 7, 9, 10, 11, 13, 15, 20, and 25 m). In practice, few monitoring locations will have this level of instrumentation.

B5 Model Evaluation

Using our simplified snowpack model, we are able to replicate the ground temperature observations reasonably well (Figure B2), corresponding with our intent of generating plausible transient ground-thermal regimes. There is some deviation from observations, notably in 2021, although we primarily attribute this to the ERA5 data overestimating winter precipitation or air temperature. Our calibrated snow parameters are (β = 365 days, γ = 20 $Wm^{-3}K^{-1}$, $\mathcal{H}_{max}$ = 15 $\mathrm{Wm^{-2}K^{-1}}$).

B6 Plausibility of simulated trends

We compare our simulation results with observed warming rates. These results are not intended to be interpreted as predictions of future permafrost warming. Rather, we perform this evaluation to ensure simulations are plausible in comparison with observed behaviour. First, we estimate yearly warming rates for MAGT at 13 m (Figure B3).

Warming rates in our simulations are distributed with a peak near 0 °C dec^{-1} and the majority of values between 0 and 0.6 °C dec^{-1}. These values include the means and confidence intervals for average warming rates reported by Biskaborn et al. (2019). Smith et al. (2022) reports maximum observed warming rates of between 0.7 and 0.9 °C dec^{-1} in various high-latitude regions of continuous permafrost. These values are also consistent with our simulations, although some of our simulations exhibit periods with greater warming rates; we attribute these to both the nature of the bedrock simulations, which have little water to buffer temperature changes, and to the fact that we are simulating a much longer period which extends well into the future with a moderately strong warming trend. We also observe some negative warming rates which we also attribute to our bedrock simulations which are both more susceptible to short-term temperature changes and under-represented in permafrost monitoring. The peak of the histogram corresponds to warming rates near 0 °C. Low warming rates (<0.1–0.3 °C dec^{-1}) are commonly observed in zones of warm permafrost (Smith et al., 2022). The relatively higher proportion of periods with such
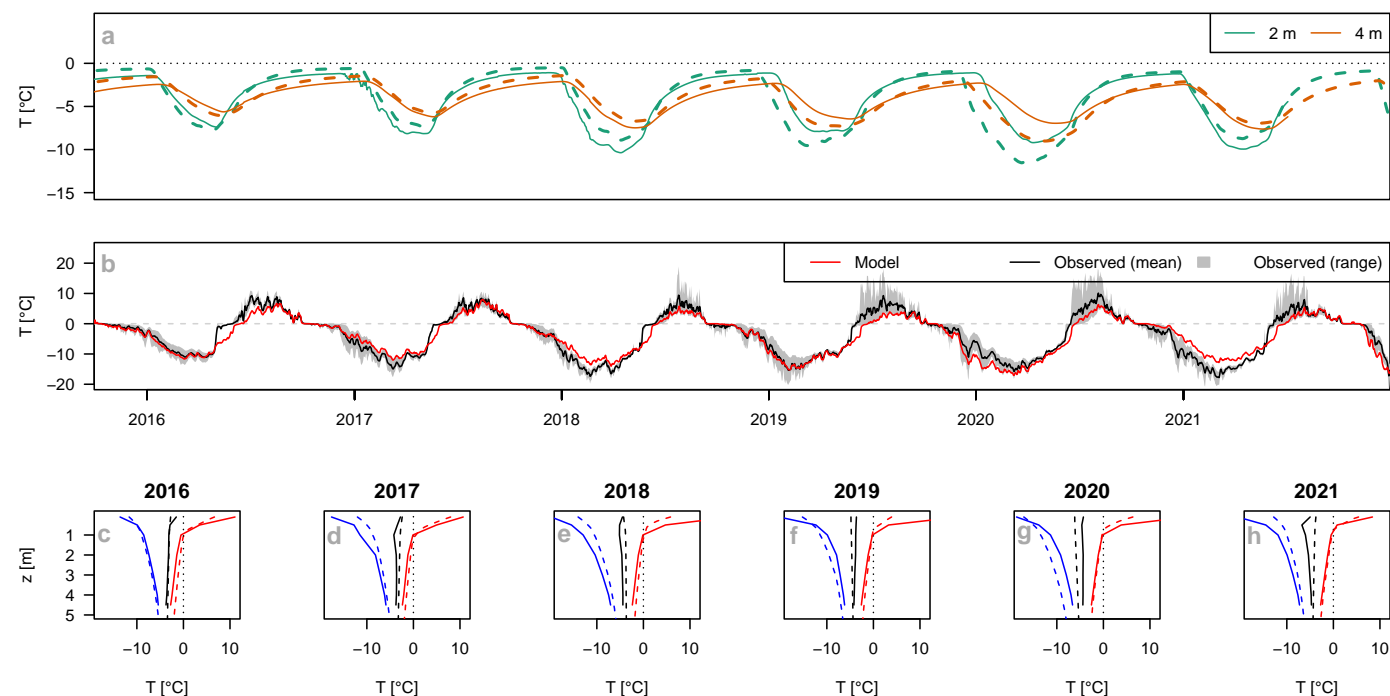
Figure B2. (a) Comparison of simulation results (dashed lines) with observations (solid lines) at selected depths (b) Comparison of simulated ground surface temperature (red) with observed mean ground temperature (black line) for 4 sensors in a 15m x 15m study plot. Grey shaded polygon shows total range. (c-h) Comparison of simulated (dashed line) and observed (solid line) temperature profiles for 2016–2021.

low rates in our simulations is also attributed to the long simulation duration and the eventual development of near-isothermal conditions in the ground for simulations with high ice contents.

Appendix C: Emulating typical sensing systems

725 In generating degraded data sets for emulating typical sensing systems (Table C1), we account for accuracy, drift, and precision for each sensor (simulation output depth). Accuracy limitations are modeled as a constant bias drawn from a uniform distribution ($\pm$ 0, 50, 150 mK). Drift is modeled as a linear trend with a slope drawn from a uniform distribution ($\pm$ 0, 1, 10 mK yr^{-1}). Precision is modeled as temporally uncorrelated normally distributed random noise (σ=0, 10, 50 mK).

Sensor accuracy of commercial systems is commonly self-reported between ± 0.005 and ± 0.4 °C. Hasler et al. (2011)
730 estimate relative sensor accuracy to be within $\pm$ 0.3 °C.

Sensor drift is reported by manufacturers between 0.002 and 0.1 °C yr^{-1}, whereas studies under laboratory conditions give much lower rates (Lawton and Patterson, 2002). However, drift is thought to also be caused by water ingress and corrosion under field conditions or by the aging of reference resistors in logging systems. Nonlinear drift has been reported in observations;
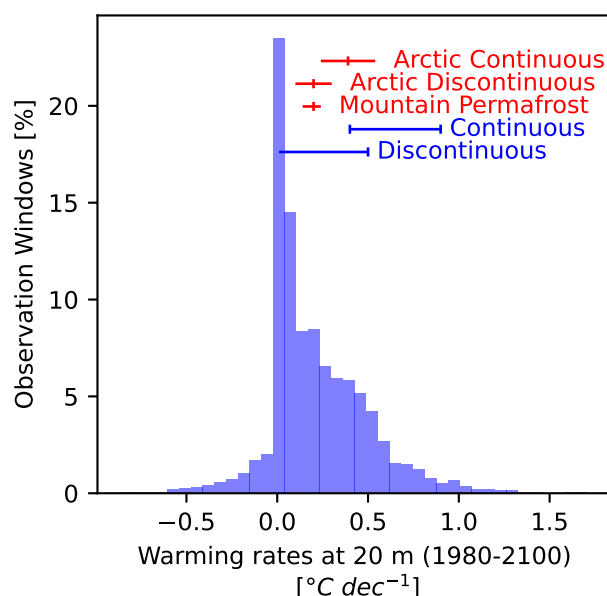
Figure B3. Histogram of warming rates at 20 m as a percentage of all possible 10-year observation windows all years across all simulations. Red intervals correspond to the mean (midpoint) and confidence interval of warming rates reported by Biskaborn et al. (2019) for different permafrost zones. Blue intervals correspond to ranges of warming rates reported in Smith et al. (2022) for different permafrost zones.

Boike et al. (2018) observe a jump of 0.5 °C over the course of a year following two years of stability and Luethi and Phillips

735 (2016) report that drifts increase exponentially with time.

Sensor resolution (precision) reported by manufacturers ranges from 0.05 mK to 63 mK. This value determines the smallest detectable change using the sensor. Widmer et al. (2023) estimated an average noise standard deviation for sensors around 5 mK (digital band-gap) and 0.03 mK (analog resistance thermistor). Batir et al. (2017) measured standard deviations around 14 mK for deep, thermally-stable sensors.

740 **Appendix D: Determination of exact active-layer thickness from model output**

The definition of the active layer can be based on phase (*frozen* or *thawed*) or temperature (*cryotic* or *non-cryotic*). As the determination of the former is more complicated and ambiguous we rely on thermal criteria to delineate the active layer.

The model FreeThawXice1D tracks and records the position of the zero-degree isotherms in the soil column. However, some post-processing is necessary to estimate the location of the active layer from this data (see example results in Fig. D1).

745 Difficulties arise due to possible existence of a supra-permafrost talik, the occurrence of additional zero-degree isotherms within the active layer, and the discontinuity of the isotherms. Our procedure for estimating ALT from the model results is as follows and uses height above a fixed datum rather than depth below the surface in its calculations.

Table C1. Sensor accuracy, resolution, and drift from manufacturer websites.

	Accuracy [mK]	Resolution [mK]	Drift [mK yr^{-1}]
CS225[1]	200 (400*)	7.8	
TNode[2]	100	10	20
TNodeHD[2]	50	0.1	10
U23-001A[3]	250	40	10
U23-003[3]	210	20	100
Concerto3Tx[4]	5	0.05	2

1. https://campbellsci.ca/cs225

2. https://thermistor-string.com/index.php/string-features#specs

3. https://onsetcomp.com/products/data-loggers/u23-004

4. https://rbr-global.com/products/standard-loggers/thermistor-strings/

All web links last accessed October 1, 2024

* Worst-case scenario including lifetime drift

Each year is treated individually. First, we determine the vertical extent of the permafrost using the model output data. If there are no depths at which the temperature is consistently below 0 °C, the ALT is undefined. Otherwise, we move on to the next step: determining whether there is an instant at which there are no isotherms above the permafrost. If this is the case, then the existence of a supra-permafrost talik is ruled out and the isotherm immediately above the permafrost is used to determine the thaw depth. If a talik cannot be ruled out, a final test is used. The maximum height of the first isotherm directly above the permafrost is compared with the minimum height of the isotherm above it. The region in between these two isotherms will be non-cryotic (and thawed). If this region has a finite thickness for the entirety of the year, that is taken as evidence of a supra-permafrost talik, and the second isotherm above permafrost is used to determine ALT. Otherwise, the first isotherm above permafrost is used.

A running 365-day minimum of the appropriate isotherm is calculated, and its value on the last day of each year is used as the exact ALT. In our analyses, it is used for comparing differing ways of interpolating ALT from $T(z,t)$ data.

Appendix E: Estimating d_{za}

The estimation of d_{za} can be done in several ways, but each has its own challenges. The most straightforward is to first calculate the annual amplitude at each sensor using the annual maximum and minimum temperatures, then identify the two sensors on either side of the 0.1 °C cutoff, and finally estimate d_{za} by linear or nearest-neighbour interpolation.

Unfortunately, this approach is not possible when observations are not sufficiently deep. Instead, the estimation of d_{za} by regression as described by (Bonnaventure et al., 2015) is a useful alternative. However, variation in apparent thermal diffusivity with depth will reduce the accuracy of the regression. Furthermore, the higher density of thermistors near the surface creates a bias towards near-surface values.
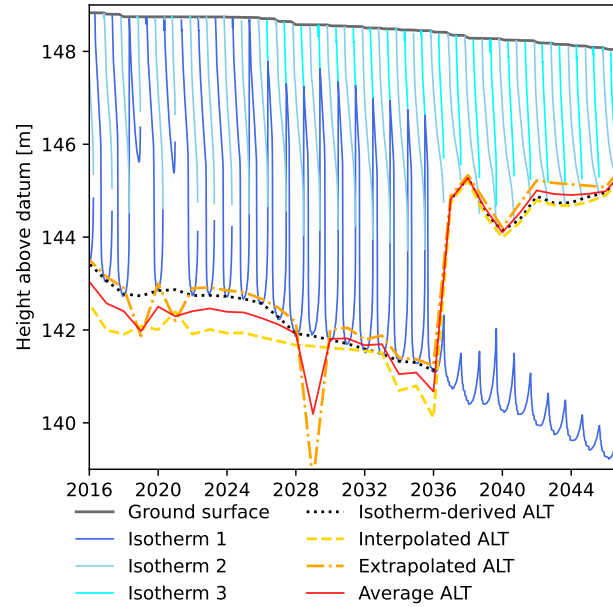
Figure D1. Example of the estimation of ALT from simulated zero-degree isotherms (blue lines) and from $T(z,t)$ model output alone (red and orange lines). This method is able to discriminate the development of supra-permafrost taliks, as shown in the years 2036–2038. However, results occasionally differ from what is expected using a purely visual inspection. For example in 2019 and 2021, the penetration depth of that year's thawing isotherm is much shallower, but because our method uses a 365-day rolling window (consistent with the definition of the active layer), the ALT for that year is relatively unchanged due to the presence of frozen ground at a greater depth in during freezeback of the previous year.

One possible solution is to modify the method of Bonnaventure et al. (2015) to use weighted regression. In this method, each (depth, amplitude) observation would be given a weighting inversely proportional to the difference between the observed amplitude and the "zero-amplitude" value of 0.1 °C. For example, weights could be calculated as

$$w_z = \frac{1}{k + |A_z - 0.1|} \tag{E1}$$

Where A_z is the amplitude at depth z, k is a constant controlling how strongly the weights diminish away from d_{za}. A strongly attenuating weighting function (small k) would more closely approximate the straightforward interpolation approach but would also work when data were missing below d_{za}.

However, we identify three additional challenges associated with the initial calculation of amplitudes at greater depths: (1) warming trends obscure small amplitude estimates, (2) phase offsets are not consistent and, (3) inter annual variability. More specifically, for small amplitudes at greater depths, warming trends impact the amplitude estimates. For example, a warming rate of 1 °C dec^{-1} can result in an increase of up to 25% in the estimated amplitude near d_{za}. Similarly, amplitudes are not always well-defined for air and ground temperature because the rising and falling limbs of the seasonal oscillation are unequal

due to the inter-annual variation in the mean and amplitude of surface air temperature. Finally, for a given yearly averaging window, amplitudes at depth have larger phase offsets than at the surface and therefore correspond to different periods. The timing of the annual extrema may differ between these periods, and it is difficult to ensure that a yearly amplitude estimates corresponds to the same surface signal at all depths.

Evaluating the various methods of calculation for d_{za} is beyond the scope of this article. However, developing an optimal strategy to reduce noise and increase d_{za} accuracy should be considered as a logical next step for the development of this metric as an indicator of permafrost change.

References

Batir, J. F., Hornbach, M. J., and Blackwell, D. D.: Ten years of measurements and modeling of soil temperature changes and their effects on permafrost in Northwestern Alaska, Global and Planetary Change, 148, 55–71, https://doi.org/https://doi.org/10.1016/j.gloplacha.2016.11.009, 2017.

Biskaborn, B. K., Smith, S. L., Noetzli, J., Matthes, H., Vieira, G., Streletskiy, D. A., Schoeneich, P., Romanovsky, V. E., Lewkowicz, A. G., Abramov, A., Allard, M., Boike, J., Cable, W. L., Christiansen, H. H., Delaloye, R., Diekmann, B., Drozdov, D., Etzelmüller, B., Grosse, G., Guglielmin, M., Ingeman-Nielsen, T., Isaksen, K., Ishikawa, M., Johansson, M., Johannsson, H., Joo, A., Kaverin, D., Kholodov, A., Konstantinov, P., Kröger, T., Lambiel, C., Lanckman, J.-P., Luo, D., Malkova, G., Meiklejohn, I., Moskalenko, N., Oliva, M., Phillips, M., Ramos, M., Sannel, A. B. K., Sergeev, D., Seybold, C., Skryabin, P., Vasiliev, A., Wu, Q., Yoshikawa, K., Zheleznyak, M., and Lantuit, H.: Permafrost is warming at a global scale, Nature Communications, 10, 264, https://doi.org/10.1038/s41467-018-08240-4, 2019.

Boike, J., Juszak, I., Lange, S., Chadburn, S., Burke, E., Overduin, P. P., Roth, K., Ippisch, O., Bornemann, N., Stern, L., Gouttevin, I., Hauber, E., and Westermann, S.: A 20-year record (1998–2017) of permafrost, active layer and meteorological conditions at a high Arctic permafrost research site (Bayelva, Spitsbergen), Earth System Science Data, 10, 355–390, https://doi.org/10.5194/essd-10-355-2018, 2018.

Bonnaventure, P., Smith, S., Riseborough, D., Duchesne, C., and Ednie, M.: The ground thermal regime across the Mackenzie Valley corridor, Northwest Territories Canada, in: GEOQuébec 2015 (68th Canadian Geotechnical Conference), Canadian Geotechnical Society, Quebec, QC, Canada, 2015.

Bonnaventure, P. P. and Lamoureux, S. F.: The active layer: A conceptual review of monitoring, modelling techniques and changes in a warming climate, Progress in Physical Geography: Earth and Environment, 37, 352–376, https://doi.org/10.1177/0309133313478314, 2013.

Brown, J., Hinkel, K. M., and Nelson, F. E.: The circumpolar activer layer montitoring (CALM) program: Research designs and initial results, Polar Geography, 24, 165–258, 2000.

Brown, N.: tsp ("Teaspoon"): a library for ground temperature data, Journal of Open Source Software, https://doi.org/https://doi.org/10.21105/joss.04704, 2022.

Brown, N., Stewart-Jones, E., Riddick, J., Meier-Legault, O., Kokelj, S., Karunaratne, K., and Gruber, S.: Air and ground temperature, air humidity and site characterization data from the Canadian Shield taiga near Yellowknife, Northwest Territories, Canada, Nordicana D, https://doi.org/10.5885/45810XD-C9F549F3E93040BD, 2022.

Brown, N., Gruber, S., Pulsifer, P., and Hayes, A.: A prototype field-to-publication data system for a multi-variable permafrost observation network, Environmental Modelling & Software, 175, 106 006, https://doi.org/10.1016/j.envsoft.2024.106006, 2024.

Burn, C. R.: The active layer: two contrasting definitions, Permafrost and Periglacial Processes, 9, 411–416, https://doi.org/10.1002/(sici)1099-1530(199810/12)9:4<411::aid-ppp292>3.0.co;2-6, 1998.

Cannon, A. J., Sobie, S. R., and Murdock, T. Q.: Bias correction of GCM precipitation by quantile mapping: How well do methods preserve changes in quantiles and extremes?, Journal of Climate, 28, 6938–6959, https://doi.org/10.1175/JCLI-D-14-00754.1, 2015.

Cao, B., Quan, X., Brown, N., Stewart-Jones, E., and Gruber, S.: GlobSim (v1.0): deriving meteorological time series for point locations from multiple global reanalyses, Geoscientific Model Development, 12, 4661–4679, https://doi.org/10.5194/gmd-12-4661-2019, 2019.

Changwei, X., Gough, W. A., Lin, Z., Tonghua, W., and Wenhui, L.: Temperature-Dependent Adjustments of the Permafrost Thermal Profiles
830   on the Qinghai-Tibet Plateau, China, Arctic, Antarctic, and Alpine Research, 47, 719–728, https://doi.org/10.1657/AAAR00C-13-128,
       2015.

Connon, R., Devoie, E., Hayashi, M., Veness, T., and Quinton, W.: The influence of shallow taliks on permafrost thaw and active layer
       dynamics in subarctic Canada, Journal of Geophysical Research: Earth Surface, 123, 281–297, https://doi.org/10.1002/2017JF004469,
       2018.

835   Cuesta-Valero, F. J., Beltrami, H., García-García, A., Krinner, G., Langer, M., MacDougall, A. H., Nitzbon, J., Peng, J., Von Schuckmann,
       K., Seneviratne, S. I., et al.: Continental heat storage: Contributions from ground, inland waters, and permafrost thawing, Earth System
       Dynamics Discussions, 2022, 1–33, 2022.

Dall'Amico, M., Endrizzi, S., Gruber, S., and Rigon, R.: A robust and energy-conserving model of freezing variably-saturated soil, The
       Cryosphere, 5, 469–484, https://doi.org/10.5194/tc-5-469-2011, 2011.

840   Devoie, E. G., Craig, J. R., Connon, R. F., and Quinton, W. L.: Taliks: A Tipping Point in Discontinuous Permafrost Degradation in Peatlands,
       Water Resources Research, 55, 9838–9857, https://doi.org/10.1029/2018wr024488, 2019.

Fourteau, K., Domine, F., and Hagenmuller, P.: Impact of water vapor diffusion and latent heat on the effective thermal conductivity of snow,
       The Cryosphere, 15, 2739–2755, 2021.

Groenke, B., Langer, M., Nitzbon, J., Westermann, S., Gallego, G., and Boike, J.: Investigating the thermal state of permafrost with Bayesian
845   inverse modeling of heat transfer, EGUsphere, 2022, 1–44, 2022.

Gruber, S.: Ground subsidence and heave over permafrost: hourly time series reveal interannual, seasonal and shorter-term movement caused
       by freezing, thawing and water movement, The Cryosphere, 14, 1437–1447, 2020.

Gruber, S., Peter, M., Hoelzle, M., Woodhatch, I., and Haeberli, W.: Surface temperatures in steep alpine rock faces - a strategy for regional-
       scale measurement and modelling, in: Proceedings of the 8th International Conference on Permafrost 2003, vol. 1, p. 325–330, Zurich,
850   Switzerland, 2003.

Gruber, S., Brown, N., Stewart-Jones, E., Karunaratne, K., Riddick, J., Peart, C., and Subedi, R.: Dense ground temperature and site charac-
       terization data from the Canadian Shield tundra near Lac de Gras, N.W.T., Canada, Earth System Science Data, 2018a.

Gruber, S., Brown, N., Stewart-Jones, E., Karunaratne, K., Riddick, J., Peart, C., Subedi, R., and Kokelj, S.: Ground temperature and site
       characterization data from the Canadian Shield tundra near Lac de Gras, N.W.T., Canada, Nordicana D, https://doi.org/10.5885/45561XX-
855   2C7AB3DCF3D24AD8, 2018b.

Gruber, S., Brown, N., Stewart-Jones, E., Karunaratne, K., Riddick, J., Peart, C., Subedi, R., and Kokelj, S.: Drill logs, visible ice con-
       tent and core photos from 2015 surficial drilling in the Canadian Shield tundra near Lac de Gras, N.W.T., Canada, Nordicana D,
       https://doi.org/10.5885/45558XX-EBDE74B80CE146C6, 2018c.

Gruber, S., Hayley, J., Karunaratne, K., King, J., MacLean, T., Marshall, S., and Moore, D.: Considerations toward a vision and strategy for
860   permafrost knowledge in Canada, 2023.

Gubler, S., Fiddes, J., Keller, M., and Gruber, S.: Scale-dependent measurement and analysis of ground surface temperature variability in
       alpine terrain, The Cryosphere, 5, 431–443, https://doi.org/10.5194/tc-5-431-2011, 2011.

Harp, D. R., Atchley, A. L., Painter, S. L., Coon, E. T., Wilson, C. J., Romanovsky, V. E., and Rowland, J. C.: Effect of soil property
       uncertainties on permafrost thaw projections: A calibration-constrained analysis, Cryosphere, 10, 341–358, https://doi.org/10.5194/tc-10-
865   341-2016, 2016.

Harris, C., Arenson, L. U., Christiansen, H. H., Etzelmüller, B., Frauenfelder, R., Gruber, S., Haeberli, W., Hauck, C., Hoelzle, M., Humlum, O., et al.: Permafrost and climate in Europe: Monitoring and modelling thermal, geomorphological and geotechnical responses, Earth-Science Reviews, 92, 117–171, 2009.

Hasler, A., Gruber, S., and Haeberli, W.: Temperature variability and offset in steep alpine rock and ice faces, The Cryosphere, 5, 977–988, https://doi.org/10.5194/tc-5-977-2011, 2011.

Hinkel, K. M.: Estimating seasonal values of thermal diffusivity in thawed and frozen soils using temperature time series, Cold Regions Science and Technology, 26, 1–15, 1997.

Hock, R., Rasul, G., Adler, C., Cáceres, B., Gruber, S., Hirabayashi, Y., Jackson, M., Kääb, A., Kang, S., Kutuzov, S., Milner, A., Molau, U., Morin, S., Orlove, B., and Steltzer, H. I.: Chapter 2: High Mountain Areas, in: IPCC Special Report on the Ocean and Cryosphere in a Changing Climate, chap. 2, pp. 131–202, Intergovernmental Panel on Climate Change, 2019.

Hu, G., Zhao, L., Li, R., Wu, X., Wu, T., Xie, C., Zhu, X., and Su, Y.: Variations in soil temperature from 1980 to 2015 in permafrost regions on the Qinghai-Tibetan Plateau based on observed and reanalysis products, Geoderma, 337, 893–905, https://doi.org/10.1016/j.geoderma.2018.10.044, 2019.

Hu, Y., Arenson, L. U., Barboux, C., Bodin, X., Cicoira, A., Delaloye, R., Gärtner-Roer, I., Kääb, A., Kellerer-Pirklbauer, A., Lambiel, C., Liu, L., Pellet, C., Rouyet, L., Schoeneich, P., Seier, G., and Strozzi, T.: Rock Glacier Velocity: An Essential Climate Variable Quantity for Permafrost, Reviews of Geophysics, 63, e2024RG000 847, https://doi.org/https://doi.org/10.1029/2024RG000847, e2024RG000847 2024RG000847, 2025.

IPCC: Summary for Policymakers, in: Climate Change 2022: Mitigation of Climate Change. Contribution of Working Group III to the Sixth Assessment Report of the Intergovernmental Panel on Climate Change, edited by Shukla, P., Skea, J., Slade, R., Khourdajie, A. A., van Diemen, R., McCollum, D., Pathak, M., Some, S., Vyas, P., Fradera, R., Belkacemi, M., Hasija, A., Lisboa, G., Luz, S., and Malley, J., Cambridge University Press, Cambridge, UK and New York, NY, USA, https://doi.org/10.1017/9781009157926.001, 2022.

Isaksen, K., Sollid, J. L., Holmlund, P., and Harris, C.: Recent warming of mountain permafrost in Svalbard and Scandinavia, Journal of Geophysical Research: Earth Surface, 112, 1–11, https://doi.org/10.1029/2006JF000522, 2007.

Kienzle, S. W.: A new temperature based method to separate rain and snow, Hydrological Processes: An International Journal, 22, 5067–5085, 2008.

Lawton, K. and Patterson, S.: Long-term relative stability of thermistors: Part 2, Precision Engineering, 26, 340–345, https://doi.org/https://doi.org/10.1016/S0141-6359(02)00110-1, 2002.

Luethi, R. and Phillips, M.: Challenges and solutions for long-term permafrost borehole temperature monitoring and data interpretation, Geographica Helvetica, 71, 121–131, https://doi.org/10.5194/gh-71-121-2016, 2016.

Meredith, M., Sommerkorn, M., Cassotta, S., Derksen, C., Ekaykin, A., Hollowed, A., Kofinas, G., Mackintosh, A., Melbourne-Thomas, J., Muelbert, M. M., Ottersen, G., Pritchard, H., and Schuur, E. A.: Polar regions, in: IPCC Special Report on the Ocean and Cryosphere in a Changing Climate, edited by Pörtner, H.-O., Roberts, D., Masson-Delmotte, V., Zhai, P., Tignor, M., Poloczanska, E., Mintenbeck, K., Alegría, A., Nicolai, M., Okem, A., Petzold, J., Rama, B., and Weyer, N., chap. 3, pp. 203–320, Intergovernmental Panel on Climate Change, https://doi.org/10.1016/S1366-7017(01)00066-6, 2019.

Nelson, F. and Hinkel, K.: Methods for measuring active-layer thickness, in: A Handbook on Periglacial Field Methods, edited by Humlum, O. and Matsuoka, N., UNIS, Longyearbyen, Norway, 2003.

Noetzli, J., Arenson, L. U., Bast, A., Beutel, J., Delaloye, R., Farinotti, D., Gruber, S., Gubler, H., Haeberli, W., Hasler, A., et al.: Best
practice for measuring permafrost temperature in boreholes based on the experience in the Swiss Alps, Frontiers in Earth Science, 9,
607 875, 2021.

905 O'Neill, H. B., Smith, S. L., Burn, C. R., Duchesne, C., and Zhang, Y.: Widespread permafrost degradation and thaw subsidence in Northwest
Canada, Journal of Geophysical Research: Earth Surface, 128, e2023JF007 262, https://doi.org/https://doi.org/10.1029/2023JF007262,
e2023JF007262 2023JF007262, 2023.

PERMOS: Swiss Permafrost Bulletin 2019 / 2020, April, Swiss Permafrost Monitoring Network (PERMOS),
https://doi.org/10.13093/permos-bull-2021, 2021.

910 Rango, A. and Martinec, J.: Revisiting the degree-day method for snowmelt computations 1, JAWRA Journal of the American Water Re-
sources Association, 31, 657–669, 1995.

Riseborough, D.: Estimating active layer and talik thickness from temperature data: implication for modeling results, in: Proceedings of the
9th International Conference on Permafrost 2008, pp. 1487–1492, Fairbanks, Alaska, USA, 2008.

Riseborough, D., Shiklomanov, N., Etzelmüller, B., Gruber, S., and Marchenko, S.: Recent advances in permafrost modelling, Permafrost
915 and Periglacial Processes, 19, 137–156, https://doi.org/10.1002/ppp, 2008.

Romanovsky, V. E., Smith, S. L., and Christiansen, H. H.: Permafrost thermal state in the polar northern hemisphere during the international
polar year 2007-2009: A synthesis, Permafrost and Periglacial Processes, 21, 106–116, https://doi.org/10.1002/ppp.689, 2010.

Sessa, R. and Dolman, H.: Terrestrial essential climate variables for climate change assessment, mitigation and adaptation, Tech. rep., Food
and Agriculture Organization of the United Nations, Rome, Italy, 2008.

920 Smith, M. W. and Riseborough, D. W.: Permafrost monitoring and detection of climate change, Permafrost and Periglacial Processes, 7,
301–309, https://doi.org/10.1002/(sici)1099-1530(199610)7:4<301::aid-ppp231>3.0.co;2-r, 1996.

Smith, S. and Brown, J.: Essential Climate Variables: Permafrost and seasonally frozen ground, Tech. rep., Global Terrestrial Observing
System (WMO/UNESCO/UNEP/ICSU/FAO), Rome, Italy, 2009.

Smith, S., Romanovsky, V., Lewkowicz, A., Burn, C., Allard, M., Clow, G., Yoshikawa, K., and Throop, J.: Thermal state of per-
925 mafrost in North America: a contribution to the international polar year, Permafrost and Periglacial Processes, 21, 117–135,
https://doi.org/10.1002/ppp.690, 2010.

Smith, S. L., O'Neill, H. B., Isaksen, K., Noetzli, J., and Romanovsky, V. E.: The changing thermal state of permafrost,
https://doi.org/10.1038/s43017-021-00240-1, 2022.

Staub, B., Hasler, A., Noetzli, J., and Delaloye, R.: Gap-filling algorithm for ground surface temperature data measured in permafrost and
930 periglacial environments, Permafrost and Periglacial Processes, 28, 275–285, https://doi.org/https://doi.org/10.1002/ppp.1913, 2017.

Stewart-Jones, E., Castagner, A., Subedi, R., Knecht, T., MacDonald, S., Macdonell, H., Jonat, G., Meier-Legault, O., Brown, N., and Gruber,
S.: Air and ground temperature, air humidity and site characterization data from the Canadian Shield taiga near Kennady Lake, Northwest
Territories, Canada, Nordicana D, https://doi.org/10.5885/45804XD-592E48652C5840F9, 2023.

Streletskiy, D., Biskaborn, B., Smith, S. L., Noetzli, J., Viera, G., and Schoeneich, P.: Strategy and Implementation Plan 2016-2020 for the
935 Global Terrestrial Network for Permafrost (GTN-P), Tech. rep., International Permafrost Association, http://library.arcticportal.org/1938/
1/GTNP_-_Implementation_Plan.pdf%0Ahttp://library.arcticportal.org/1938/1/GTNP_-_Implementation_Plan.pdf, 2017.

Subedi, R., Kokelj, S. V., and Gruber, S.: Ground ice, organic carbon and soluble cations in tundra permafrost soils and sediments near a
Laurentide ice divide in the Slave Geological Province, Northwest Territories, Canada, The Cryosphere, 14, 4341–4364, 2020.

Swiss Permafrost Monitoring Network: Swiss Permafrost Bulletin 2023, https://doi.org/10.13093/PERMOS-BULL-2024, 2024.

940 Tubini, N. and Gruber, S.: Simulating soil heat transfer with excess ice, erosion and deposition, guaranteed energy conservation, adaptive mesh refinement, and accurate spin-up (FreeThawXice1D), The Cryosphere, https://doi.org/10.5194/egusphere-2025-2649, submitted, 2025.

Tubini, N., Gruber, S., and Rigon, R.: A method for solving heat transfer with phase change in ice or soil that allows for large time steps while guaranteeing energy conservation, The Cryosphere, 15, 2541–2568, https://doi.org/10.5194/tc-15-2541-2021, 2021.

945 van Everdingen, R. O.: Multi-language glossary of permafrost and related ground-ice terms, National Research Council of Canada. Associate Committee on Geotechnical Research. Permafrost Subcommittee, https://doi.org/https://nsidc.org/cryosphere/glossary-terms/frozen-ground-or-permafrost, 1998.

Von Schuckmann, K., Minière, A., Gues, F., Cuesta-Valero, F. J., Kirchengast, G., Adusumilli, S., Straneo, F., Ablain, M., Allan, R. P., Barker, P. M., et al.: Heat stored in the Earth system 1960–2020: where does the energy go?, Earth System Science Data, 15, 1675–1709,
950 2023.

Wang, Q., Okadera, T., Watanabe, M., Wu, T., and Ochirbat, B.: Ground warming and permafrost degradation in various terrestrial ecosystems in northcentral Mongolia, Permafrost and Periglacial Processes, 33, 406–424, https://doi.org/https://doi.org/10.1002/ppp.2161, 2022.

Wang, S., Cao, B., Hao, J., Sun, W., and Zhang, K.: Consistent ground surface temperature climatology over China: 1956–2022, Journal of Geophysical Research: Atmospheres, 129, e2024JD040 916, https://doi.org/https://doi.org/10.1029/2024JD040916, e2024JD040916
955 2024JD040916, 2024.

Widmer, L., Phillips, M., and Buchli, C.: Brief communication: Comparison of the performance of thermistors and digital temperature sensors in a mountain permafrost borehole, The Cryosphere, 17, 4289–4295, https://doi.org/10.5194/tc-17-4289-2023, 2023.

Wu, Q. and Zhang, T.: Changes in active layer thickness over the Qinghai-Tibetan Plateau from 1995 to 2007, Journal of Geophysical Research: Atmospheres, 115, https://doi.org/https://doi.org/10.1029/2009JD012974, 2010.

960 Wu, T., Zhao, L., Li, R., Wang, Q., Xie, C., and Pang, Q.: Recent ground surface warming and its effects on permafrost on the central Qinghai-Tibet Plateau, International Journal of Climatology, 33, 920–930, https://doi.org/10.1002/joc.3479, 2012.